NASA CR-144375
MDC E1249
NASA CR-

PARTICULATE CONTAMINATION SPECTROMETER

by

R.J. SCHMITT, B.A. BOYD AND R.M.F. LINFORD

MCDONNELL DOUGLAS ASTRONAUTICS COMPANY - EAST

Saint Louis, Missouri

Contract NAS9-14171

May 1975

FINAL REPORT

VOLUME I TECHNICAL REPORT

prepared for

NATIONAL AERONAUTICS AND SPACE ADMINISTRATION

LYNDON B. JOHNSON SPACE CENTER

1. Report No.	2. Government Accession No.	3. Recipient's Catalog No.

4. Title and Subtitle	5. Report Date
PARTICULATE CONTAMINATION SPECTROMETER, VOLUME I, TECHNICAL REPORT	May 1975
	6. Performing Organization Code
7. Author(s)	8. Performing Organization Report No.
R. J. Schmitt, B. A. Boyd and R. M. F. Linford	MDC E1249
	10. Work Unit No.
9. Performing Organization Name and Address	
McDonnell Douglas Astronautics Company - East St. Louis, Missouri 63166	11. Contract or Grant No. NAS9-14171
	13. Type of Report and Period Covered Contractor Report July 1974 - March 1975
12. Sponsoring Agency Name and Address	
National Aeronautics and Space Administration Washington, D. C. 20546	14. Sponsoring Agency Code

15. Supplementary Notes

Contracting Officer Representative, R. G. Richmond, NASA Johnson Space Center, Houston, Texas

16. Abstract

ABSTRACT

A Laser Particulate Spectrometer (LPS) System was developed to measure the size and speed distributions of particulate (dusts, aerosols, ice particles, etc.) contaminants. Detection of the particulates is achieved by means of light scattering and extinction effects using a single laser beam to cover a size range of 0.8 to 275 microns diameter and a speed range of 0.2 to 20 meter/second. The LPS System was designed to operate in the high vacuum environment of a space simulation chamber with cold shroud temperatures ranging from 77 to 300°K.

17. Key Words (Suggested by Author(s))	18. Distribution Statement
Particle Size Distribution Aerosol Size Laser Scattering Laser Extinction MIE Scattering	Unclassified - Unlimited

19. Security Classif. (of this report)	20. Security Classif. (of this page)	21. No. of Pages	22. Price*
Unclassified	Unclassified	78	

*For sale by the National Technical Information Service, Springfield, Virginia 22151 Copy No. _____

NASA — JSC

FOREWORD

This final report was prepared by McDonnell Douglas Astronautics Company - East, under NASA Contract NAS9-14171 and covers work performed during the period July 1974 to March 1975. This work was administered under the direction of NASA Johnson Space Center with Robert G. Richmond as the Contracting Officer Representative. The Program Manager was Dr. R. M. F. Linford with R. J. Schmitt and B. A. Boyd being responsible for the technical effort. Acknowledgement is given to the valuable contributions made by T. H. Allen and A. C. Lind, program consultants; J. E. Wittman, design; J. Sneed and E. Walters, fabrication.

This report is in two volumes:

Volume I - Technical Report

Volume II - Operating Instructions

ABSTRACT

A Laser Particulate Spectrometer (LPS) System was developed to measure the size and speed distributions of particulate (dusts, aerosols, ice particles, etc.) contaminants. Detection of the particulates is achieved by means of light scattering and extinction effects using a single laser beam to cover a size range of 0.8 to 275 microns diameter and a speed range of 0.2 to 20 meter/second. The LPS System was designed to operate in the high vacuum environment of a space simulation chamber with cold shroud temperatures ranging from 77 to 300°K.

TABLE OF CONTENTS

LIST OF PAGES

TITLE PAGE

LIST OF ILLUSTRATIONS

1.0 INTRODUCTION

The increasing complexity of space-vehicle designs and experiment payloads, coupled with increasing mission durations, has resulted in stringent cleaniness requirements for space environmental testing and simulation facilities. It is well known that particulates or dust are found in the large, high vacuum chambers used in space simulation and that they may constitute a source of contamination to test articles placed inside these chambers[1]. Since it becomes increasingly expensive to maintain high quality clean room environments of large dimensions, studies have been conducted [2,3] to determine the history of the suspended particulates in a space simulation chamber during the entire cycle of thermal-vacuum testing, viz, pretest (atmospheric), early pumpdown, high vacuum, chamber repressurization, and post-test (atmospheric).

These studies pointed out the necessity for an instrument, which can measure and display in a convenient way (e.g. CRT oscilloscope, x-y plotter) the distributions of particle sizes and speeds. With such an instrument the details of the total behavior of particulate distributions can be defined.

This report contains a description of the design, fabrication and performance of a Laser Particulate Spectrometer (LPS) System. This instrument measures the size and speed distributions of particulates (dusts, aerosols, ice particles, etc.) passing through the laser beam by detecting both the light scattered by the smaller particles, and the laser beam intensity fluctuations due to larger particles. Details are presented of the system design which resulted in the development of an instrument sensitive to particles

from 0.8 to 275μm diameter moving through the laser beams at speeds between 0.2 to 20m/sec. A significant feature of the LPS design is the capability for operation at pressures ranging from room ambient to ultra-high vacuum and for operation within vacuum chamber cold shrouds which range in temperature from 77 to 300°K.

The LPS System is designed to be compatible with Hewlett-Packard 5401B/9810 Multi-Channel Analyzer/Programmable Calculator System. The LPS Electronics System was designed and assembled as part of this program to provide the required compatibility. Special computer programs were developed to permit automatic acquisition and recording of LPS data (via digital cassette tape and X-Y Plotter).

This program was conducted in three phases. Upon completion of Phase I, in which a review of available techniques for particulate sizing was made, it was concluded that laser scattering and extinction methods offered the best approach for the requirements of this program.

Phase II involved a detailed design study of the dual-mode laser scattering and extinction spectrometer. At the completion of the Phase II effort, a Design Review was held and it was agreed that the single-beam design should be optimized for particulates in the 1 to 100μm diameter range. The Laser Particulate Spectrometer (LPS) which was delivered to NASA actually operated from 0.8 to 275μm diameter.

The Phase III effort involved the detailed design, fabrication, calibration and delivery of the LPS System.

This report consists of two volumes. Volume I is the Technical Report which contains six sections. Section 1.0 is introductory material. Section 2.0 presents the results of a study undertaken at the onset of this program to determine which of the many available techniques for particle sizing was

best suited for the present requirements. Section 3.0 includes details of the optical, mechanical, thermal and electronic design of the LPS. Section 4.0 presents details of the LPS instrument which was ultimately fabricated, of the system operational procedure and of the system calibration tests. Section 5.0 contains conclusions and recommendations, while Section 6.0 contains an extensive bibliography on the theory and techniques of particle size measurement.

Volume II contains the Operations Manual for the LPS System and details the computer software developed for the LPS system.

2.0 TECHNIQUE SELECTION

The first task in the program involved the retrieval of applicable theoretical and empirical data from the literature on particle sizing techniques. The resources of the McDonnell Douglas Mechanized Information Retrieval Service were used to assemble the applicable references, a detailed compilation of which is found in Section 6. In this section a summary of the results of this study is presented. Optical techniques were established as offering the best possibilities for achieving the aims of this program. An analysis of several optical techniques is presented, after which the selected design approach is detailed.

2.1 LITERATURE SURVEY. An examination of the documents retrieved in the literature survey revealed a variety of methods for particle counting, sizing and velocity determination. Information was also found on a number of instruments that could be applied to one or several of the requirements of this program. A preponderance of methods based on optical techniques was noted. Since the system to be realized had to function in a simulated space environment, an effort was made to uncover those methods and equipment used to measure particulate fluxes on spacecraft, and to evaluate the usefulness of these methods in light of the program requirements.

2.1.1 EMISSION SPECTROSCOPY. Nothing was found in the literature to suggest that techniques based on emission spectroscopy could be successfully applied to sizing small particles (0.1-500μm diameter) in a vacuum chamber. Heating particles to produce emission of radiant flux is limited by the very

low radiance levels produced. Consequently it was decided that it was not profitable to pursue this technique.

2.1.2 HOT WIRE ANEMOMETRY. Several references were uncovered in which specially designed hot wire anemometer probes were used to measure the properties of a two phase gas-aerosol flow. It was clear from a study of these references that, although one can detect the impingement of an aerosol particle on the hot wire, the pulses produced thereby are extremely difficult to interpret in terms of particle size (mass). In addition, since the method is essentially destructive to the aerosol particle, velocity determination by this method is precluded. In a telephone conversation with a leading manufacturer of hot wire equipment, (Thermo-Systems, Inc., St. Paul, Minnesota), it was pointed out that hot wire probes are extremely fragile when designed for fast response and are easily damaged by the impact of solid or liquid particles. On the basis of these considerations hot wire anemometry was eliminated as a viable technique for the program.

2.1.3 ACOUSTICAL TECHNIQUES. Several references were located in the literature which describe acoustical techniques applied to the detection of micro-meteorite impacts. Devices based on this technique have been flown on numerous space vehicles. While they perform admirably as particle counters to determine particle fluxes, it was clear that extracting information on the distribution of particle sizes using acoustical techniques alone is not straightforward. These detectors produce output amplitudes which are proportional to particle kinetic energy or momentum. Such detectors have demonstrated the capability to count micron-size solid particles travelling at relative speeds of several km/sec, but no evidence could be found in the literature that this technique can be applied to liquid particles moving at a few meters/sec.

For these reasons this method was not further pursued.

2.1.4. ELECTROSTATIC TECHNIQUES. The literature search revealed several references describing electrostatic methods for particle sizing. Since sizable electric field strengths are required in this technique (400-10,000 volts/cm), the possibility of corona discharge occurring in some pressure range during chamber pumpdown would be appreciable. No evidence was found in the literature that electrostatic techniques have been used to size particles in the range required in a vacuum chamber. As signal levels tend to be low (~1 microvolt), special precautions are required to eliminate electrical noise from the system. We concluded that the corona problem is sufficiently serious to eliminate this method from further consideration.

2.1.5 OPTICAL TECHNIQUES. The majority of the references retrieved via the literature search describe what might be summarily termed "optical techniques for particle diagnostics". Included under this heading are methods based on the scattering of light by a particle, interruption of a light beam by a particle (extinction), techniques of imaging small particles (microscopy, ultramicroscopy, and holography), polarization methods of particle measurement, optical time of flight measurements, and laser doppler velocimetry (LDV) techniques. A single common characteristic which commends such techniques for the present program is that they all probe a particle distribution in a non-descructive manner via a beam of light. Additionally, the literature reveals that several approaches based on optical techniques have reached a high state of development and, with appropriate modifications and further development, could be adapted to the goals of the present program.

2.1.6 LASER DOPPLER VELOCIMETRY. A number of references describing methods of Laser Doppler Velocimetry (LDV) were retrieved in the literature search. This technology has evolved during the past ten years from a purely laboratory technique to the point where several vendors can supply various types of instrumentation. Although LDV has been principally used to determine velocity components of particle-seeded gas flows (e.g., wind tunnel applications), recent attempts have been described to extend LDV to particle counting and sizing problems. LDV systems consist of a single laser beam which is split into two or more beams which are subsequently crossed to produce a localized probe volume. A one or two dimensional set of interference fringes is formed in the probe volume. Light scattered out of the probe volume by the particle is directed onto a detector to produce an output which, in general, appears as a pulse with superimposed high frequency ripple. The low frequency hump, the pedestal, is due to the usual Gaussian intensity distribution which characterizes the fringe system in the probe volume. The high frequency component is the Doppler signal, the frequency of which is directly related to one or more velocity components of the particle. A spectrum analyzer or tracking filter is commonly used to extract the frequency of the Doppler signal from the composite output. The visibility function defined as

$$V = \frac{V_1 - V_2}{V_1 + V_2} \qquad (2.1)$$

where (V_1-V_2), the amplitude of the high frequency ripple, is related to the particle size. Some progress has been made recently in relating the visibility V to particle size in the 10 to 120μm diameter range. Extension of this

approach to smaller particle sizes has proven to be difficult because of the resulting small values of V which characterize these smaller particles. This problem is accompanied by a further difficulty of the need for specialized and expensive electronic systems to process the visibility data. In the communication with TSI mentioned above, this vendor indicated that they are presently working on the application of LDV methods to particle sizing and that they are a year or more away from producing a marketable system. Since the LDV method is an extra-cavity rather than intra-cavity method, rather high power lasers (typically 100mW) are required. This is expected to exacerbate the thermal problems associated with operation of such lasers in a vacuum chamber. We concluded that LDV techniques will require substantial development before they are optimized for small particles (<10μm diameter) and since there are other optical methods with proven capability for sizing small particles, we should concentrate on the latter.

2.1.7 VACUUM QUALIFIED LASERS. The literature search revealed several reports describing the design and development of a space-qualified helium-neon (He-Ne) laser by Hughes Electron Dynamics Company. This topic was significant to the program since any candidate technique which relies on a laser could involve operating a laser in hard vacuum. The Hughes space-qualified laser represents a considerable refinement in both design and materials over commonly available commercial lasers.

2.1.8 AEROSOL GENERATION. Early in the development of the LPS, it was realized that some method of generating an aerosol for demonstration and calibration purposes was required. For this reason, references describing various methods of aerosol generation were accumulated. Those techniques investigated

include ultrasonic nebulizers, electrostatic nozzles, various smoke generators and methods of separating and dispersing dry solid particles. The methods used in this program for aerosol generation are detailed in Section 4.4

2.2 ANALYSIS OF OPTICAL TECHNIQUES.

2.2.1 FAR-FIELD DIFFRACTION PATTERNS. The techniques of optical imaging, microscopy and holography, require knowledge of the diffraction patterns produced by a particle as it moves through a light beam. Computer codes were written for this program which predict these patterns for arbitrarily sized particles using Kirchhoff Diffraction Theory. Both coherent (laser) and non-coherent illumination conditions were studied. This study was restricted to far-field or Fraunhofer diffraction patterns since these are basic to holographic techniques and since it is relatively easy to compute the intensity distribution of these patterns. Figure 2-1 shows typical far-field intensity distributions produced by an opaque spherical particle illuminated by collimated beams of both coherent (laser) and incoherent light. The intensity in the diffraction pattern normalized to the intensity of the undisturbed incident light is plotted as a function of radial distance in an observation plane oriented normal to the direction of the incident light for several far-field distanced (FFD) from the particles. The FFD is defined by

$$Z^* = \frac{4a^2}{\lambda} \qquad (2.2)$$

where a = particle radius

λ = wavelength of the incident light.

Z^* is the distance at which the diffraction pattern changes from the Fraunhofer type to the Fresnel, or near-field, diffraction pattern.

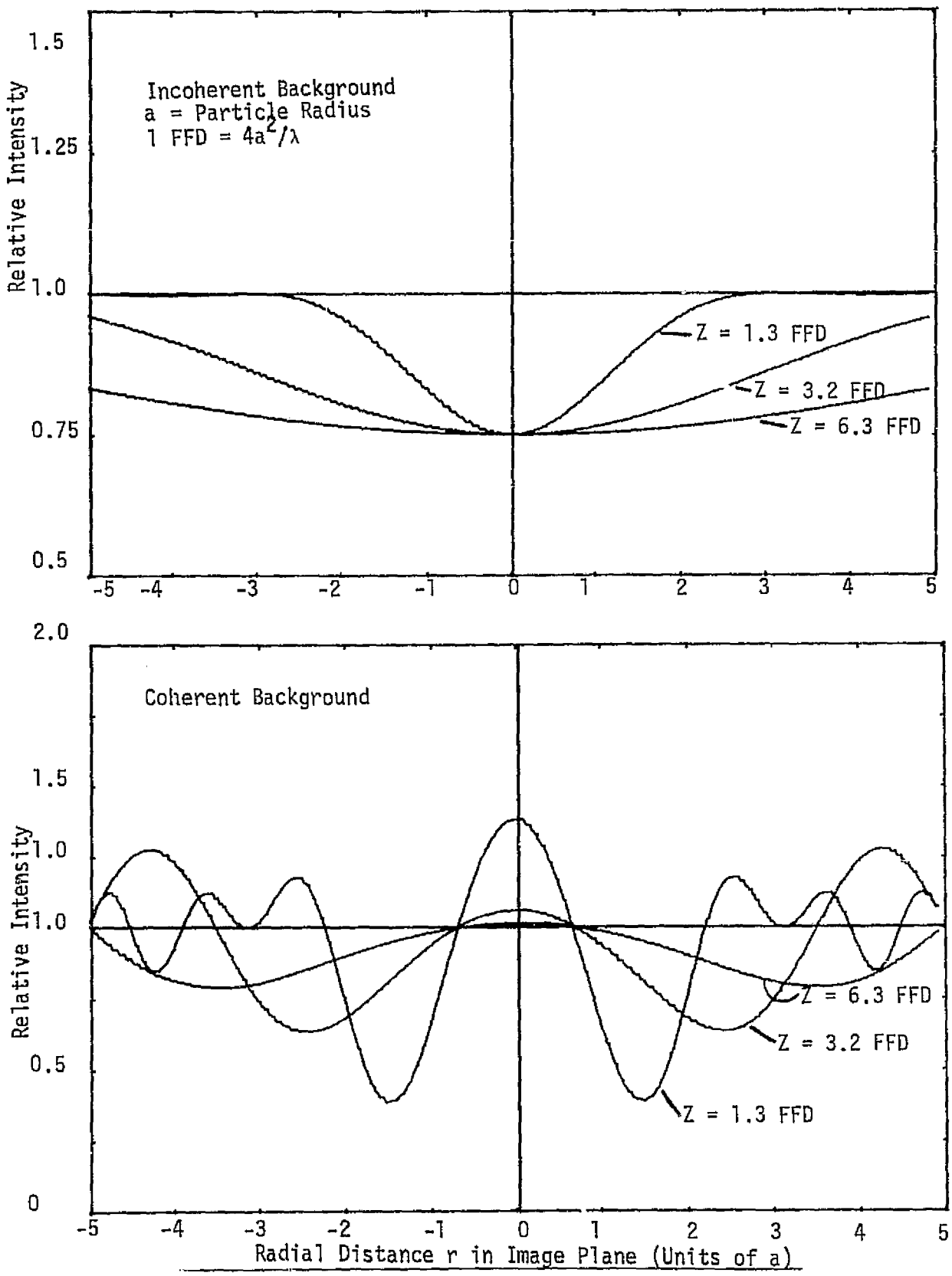

FIGURE 2-1 - FRAUNHOFER DIFFRACTION PATTERNS

With an incoherent background, the far-field pattern shows a dark spot centered the axis of the incident light beam ($r = 0$) which approaches the geometrical shadow of the spherical particle (diameter = $2a$) as the far-field distance, Z, decreases. This implies that with incoherent background light one must work in the near-field, or Fresnel, diffraction region, in order to measure particle size by means of shadows.

For the case of coherent background illumination, a Fraunhofer hologram of the particle is observed in the far-field region (see Figure 2-1). In contrast to the incoherent case, a central bright spot appears in the diffraction pattern centered on the axis of the incident light ($r = 0$). Figure 2-1 shows the intensity variations in the diffraction patterns formed with coherent light for three FFD's. The width of this central bright spot, or Airy disk, is given by

$$2r_A = \frac{1.22Z\lambda}{a} \qquad (2.3)$$

where r_A = Airy disk radius

Z = distance between particle and plane of observation

a = particle radius

Equation 2.3 essentially defines the diameter of the Airy disk in the diffraction pattern and relates it to particle size.

Figure 2-2 shows the variation in the relative intensity distribution in an image plane 2cm from the particle for 20, 50, and 100μm diameter particles. For such diffraction patterns, the intensity of the rings is dependent on particle size but the radius of the first dark ring is not.

Figure 2-3 shows the relation of particle diameter to the diameter $2r_A$ of the Airy disk as a function of far-field distance Z. The dashed curve is

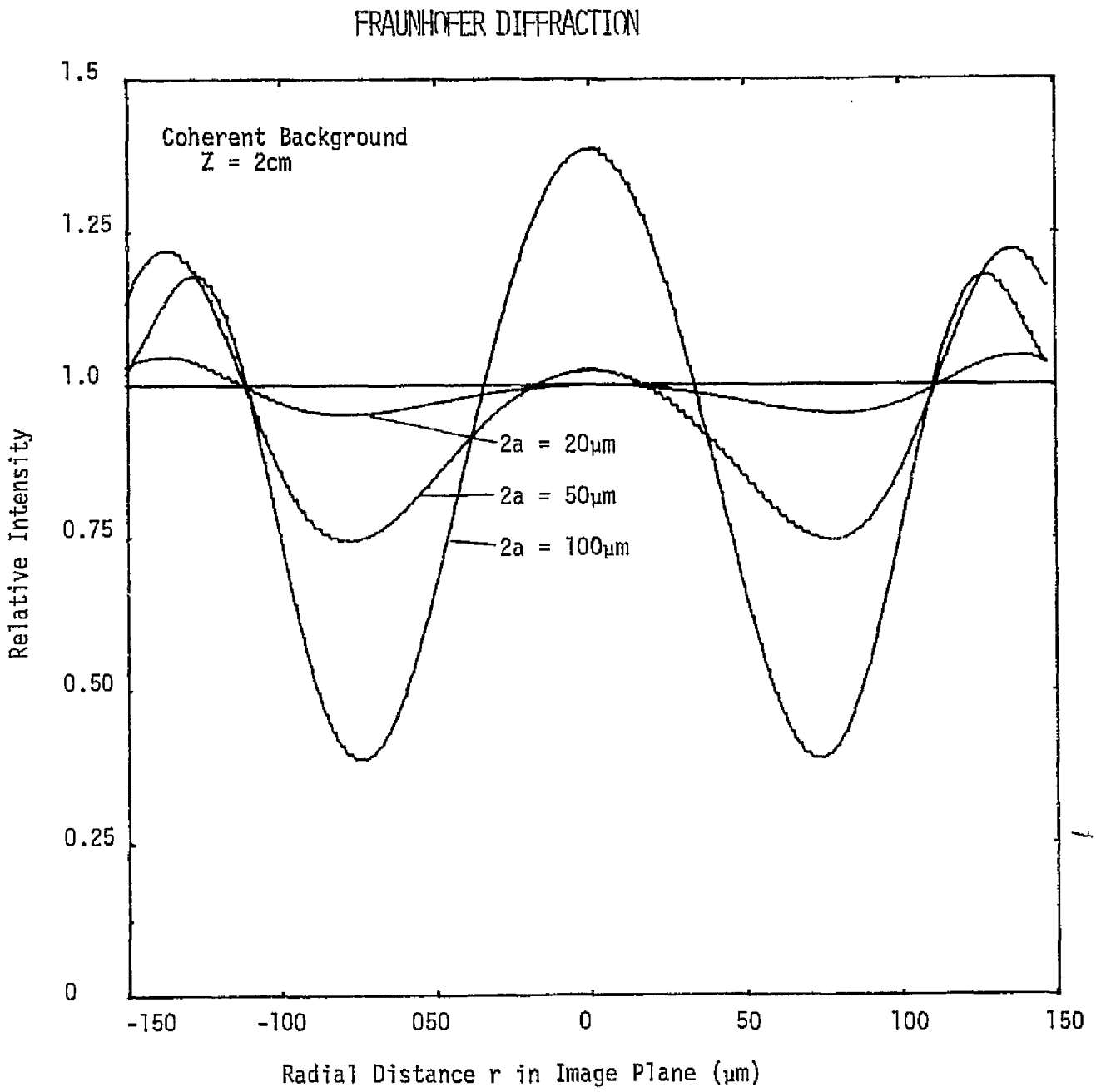

FIGURE 2-2 - FRAUNHOFER DIFFRACTION PATTERNS AT Z = 2cm

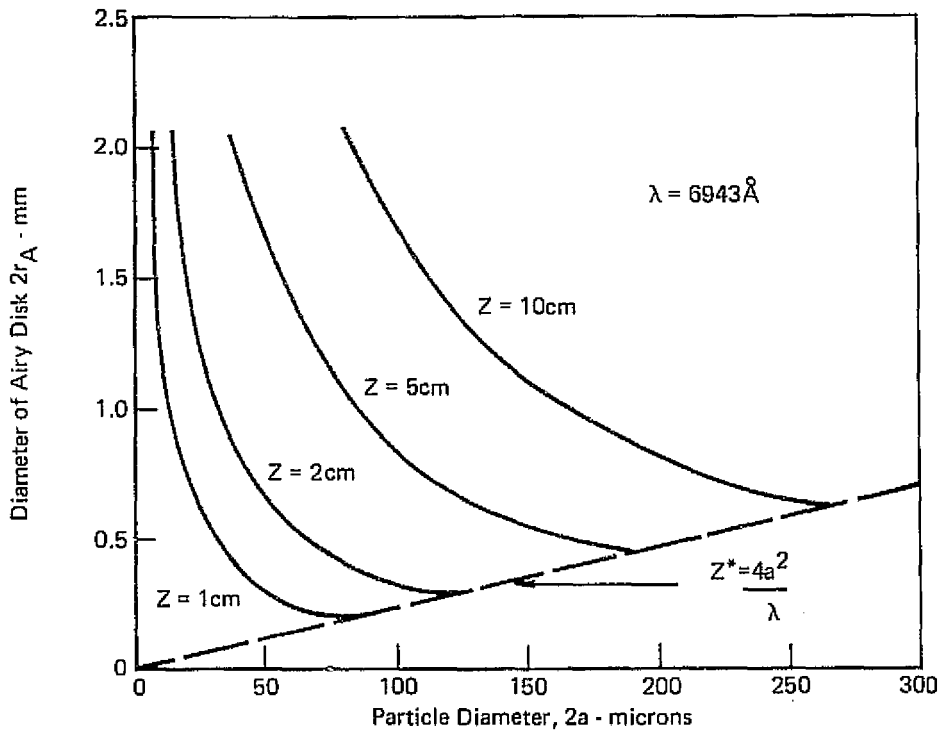

FIGURE 2-3 – DIAMETER OF FIRST MINIMUM OF AIRY PATTERN VERSUS PARTICLE DIAMETER

a plot of the far-field condition given by Equation 2.2 and limits the range of particle diameter to which Equation 2.3 applies for a given far-field distance. In general small values of far-field distance Z are associated with high contrast between the bright and dark fringes in the diffraction pattern. This is desirable because it simplifies the measurement of the Airy disk diameter. However, a penalty is paid because of the reduced range of particle sizes which can be accommodated and the loss of sensitivity for small particles diameters, as is evident in Figure 2-3 for Z = 1cm, where the slope of the curve becomes very steep for $2a \leq 25$ microns. Conversely, by working at larger far-field distances we increase the range of particle sizes which can be

measured, but the diffraction patterns show a marked decrease in contrast between bright and dark fringes (see Figure 2-1) for coherent illumination.

While it is evident from this analysis that imaging techniques can be used to size particles greater than 5 microns diameter, there is a severe problem common to such techniques when applied to small, fast moving particles. For example, a 5 micron diameter particle moving at 50m/sec travels a distance equal to its diameter in 10^{-7} sec. In an imaging system this is the available time for measuring the diameter of the Airy disk. Thus a severe impact on the design of the electronics system results. In Section 2.2.3 the alternative method of laser extinction is shown to minimize the requirement for high speed electronics for sizing particles larger than 10 microns diameter.

2.2.2 PARTICLE SIZING BY MIE SCATTERING. The literature survey revealed numerous applications of scattering techniques for sizing particles less than 10 microns diameter. To study the sensitivity of optical scattering methods, Mie scattering programs were written for a H-P 9830 Calculator and for a CDC 6500 computer. In addition to calculating the scattered intensity for particles in an ordinary light beam, a modification of the programs allowed the computation of the scattered intensity for a particle located in the cavity beam of a laser.

Besides having the obvious advantage of increasing the incident power on the particle, operating within the laser cavity alters the distribution of the radiation scattered by the particles, allowing greater differences between particle sizes to be detected, and increasing the scattered radiation for a given beam intensity. Examples of the intensity distributions for ordinary scattering and cavity scattering are shown in Figures 2-4 and 2-5. In both figures the logarithm of the scattered power is plotted radially at

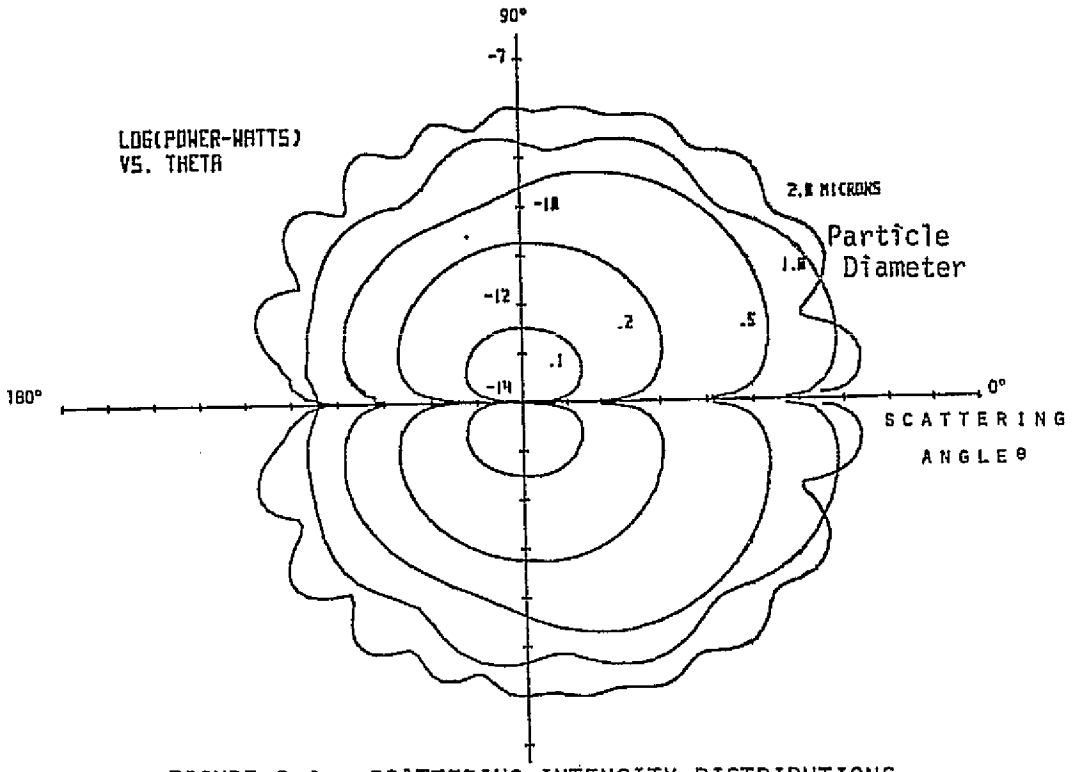

FIGURE 2-4 - SCATTERING INTENSITY DISTRIBUTIONS
(OUTSIDE LASER CAVITY)

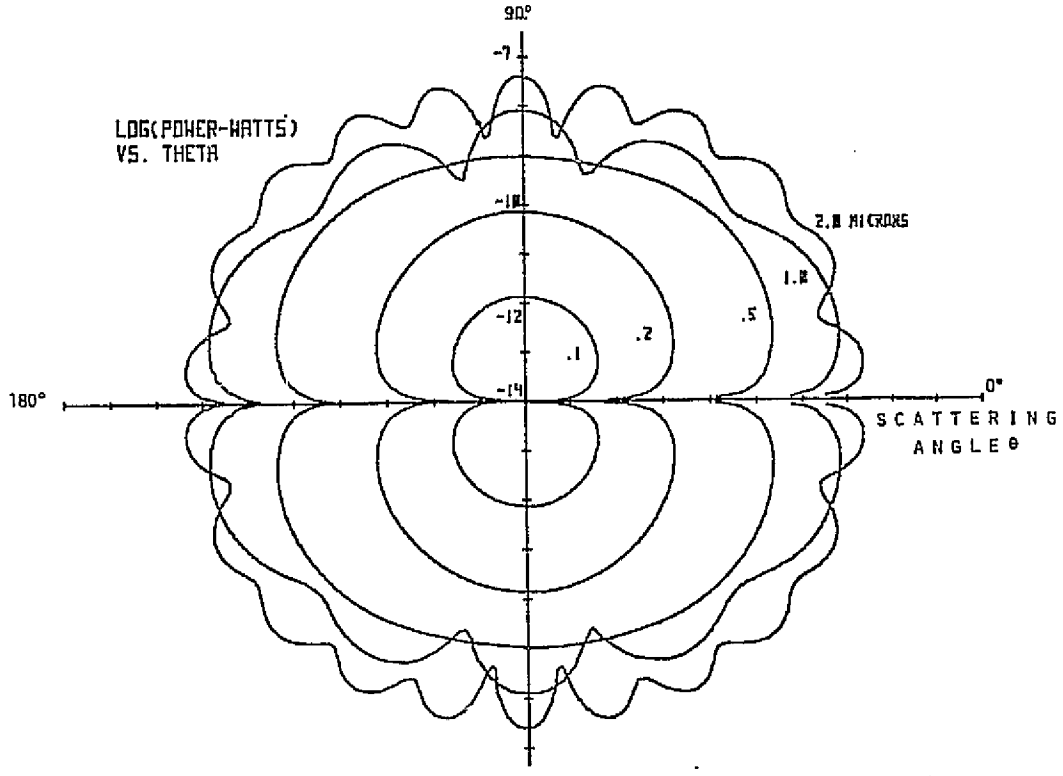

FIGURE 2-5 - MIE SCATTERING INTENSITY DISTRIBUTIONS
(INSIDE LASER CAVITY)

each scattering angle. In all cases the incident beam is assumed to have an intensity of 10^6 Wm^{-2}. It should be noted that for cavity scattering the pattern is symmetric about $\theta = 90°$ thus allowing simultaneous collection of the forward and backward scatter components to increase the collected power.

Figure 2-6 shows the optical geometry for collecting the light scattered from a particle. The collection angle is determined by the solid angles subtended by the laser mirrors and the collecting lens.

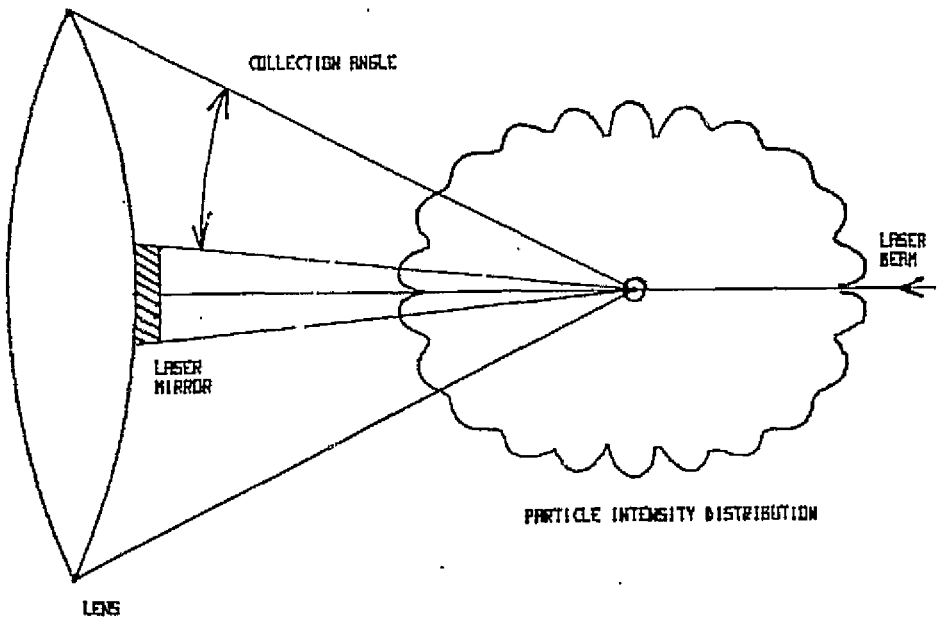

FIGURE 2-6 - LASER CAVITY SCATTERING OPTICAL GEOMETRY

Collected power from the particle for different collection angles was calculated and plotted. Figure 2-7 shows the collected power as a function of particle diameter for three collection angles. Again the incident intensity is $10^6 Wm^{-2}$. Clearly, the larger the collecting angle the more light is collected and the smoother the curve. A simple lens system was preferred over the integrating sphere and hemispherical mirror collection systems reported in the literature because the lens offers the least obstruction to the particles crossing the laser beam.

The noise-equivalent power of a typical silicon photo detector is about 10^{-9} W(2MHz band width) which sets a lower limit of about 0.2μm for the detected particles for the assumed intensity of 10^6 Wm^{-2}.

The results of the Mie scattering analysis revealed the feasibility of sizing particles ranging from 0.2 to 10 microns diameter using a simple laser system and a silicon photodiode detector to measure the light scattered by the particle from the intracavity laser beam.

2.2.3 LASER CAVITY EXTINCTION. Concurrent with the Mie Scattering analysis, a study was conducted to investigate the effects of large particles passing through a laser cavity beam. The laser cavity beam provides a very intense source of light and acts as an efficient amplifier of disturbances in the resonant cavity.

Particles passing through the laser cavity beam produce two effects: Mie scattering as described in the previous section and laser extinction. Particle sizing via Mie Scattering is a viable technique for particle sizes small enough to produce negligible perturbation of the laser cavity beam. Larger particles produce non-negligible disturbances in the laser cavity which can be used as a method for sizing such particles.

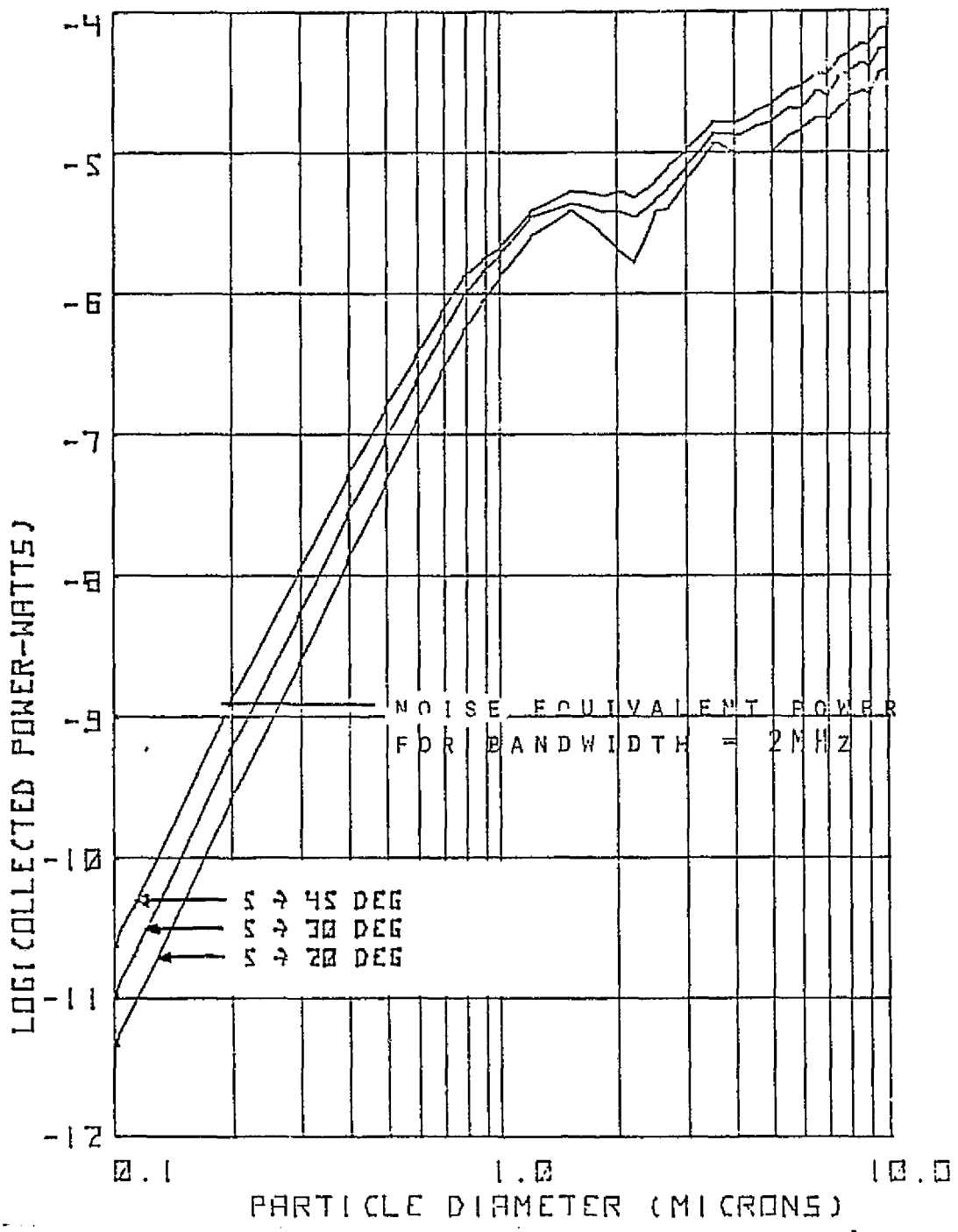

FIGURE 2-7 - LASER CAVITY SCATTERING COLLECTED POWER

Computer programs were written to compute the effects of laser and particle parameters on laser cavity extinction. Figure 2-8 shows the laser output power as a function of particle diameter for a number of beam waist radii. As can be seen, a beam radius of 100μm will allow detection and sizing of particles from about 1μm to 20μm diameter.

The same type of analysis was used to determine the shape of the extinction pulse as a particle traverses the laser beam. Figure 2-9 illustrates the laser output power as a function of time for various particle diameters crossing through the center of a 100μm radius beam at $2ms^{-1}$. The difference in pulse height for each particle size is shown along with the peak in the center as the particle crosses the dark spot of the TEM_{01*} mode. Figure 2-10 shows the effect of one size particle crossing the beam at different off-axis distances. Up to a distance of 70μm from the center (the distance to the peak of the TEM_{01*} mode pattern) the pulse height is constant for a given particle size. In addition, the time difference between the peaks can be used to determine time of flight (TOF) velocity information.

Consideration was given to a hybrid laser scattering and extinction system. Because of the complimentary nature of the phenomena of scattering and extinction, they are well suited to simultaneous use in a laser system. A scattering detector responds to small particles (0.2 to 10μm) while an extinction detector responds to larger ranges (10-100μm) within the same laser cavity probe volume. The optimum parameters for such a hybrid system are detailed in Section 3.0.

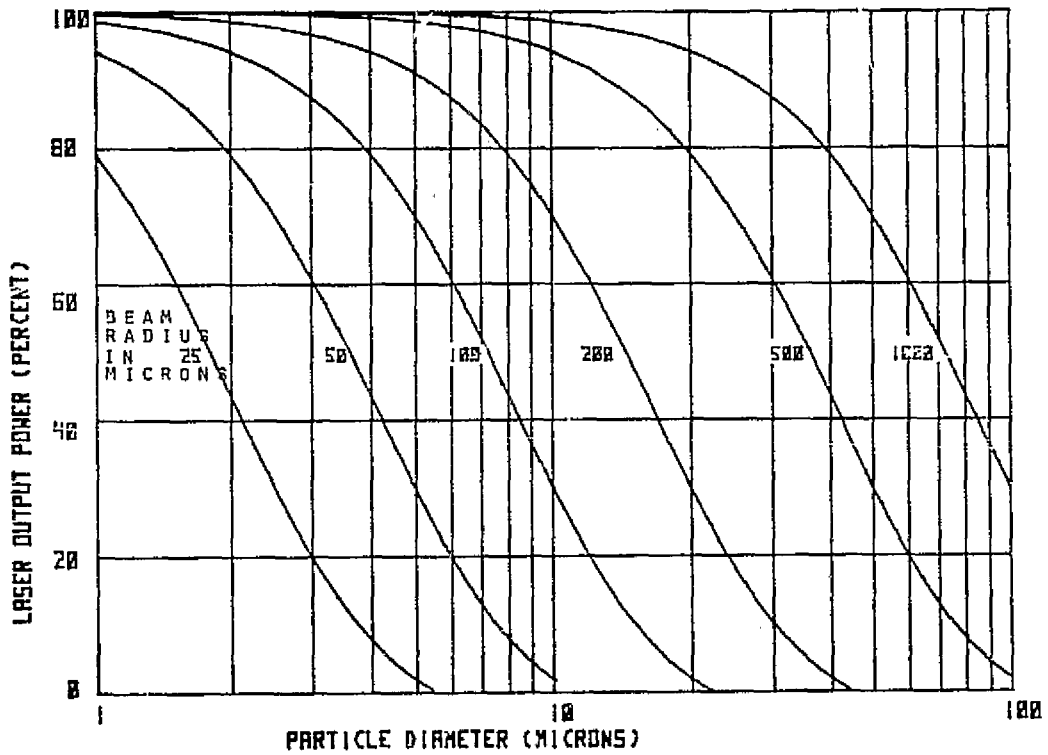

FIGURE 2-8 - LASER CAVITY EXTINCTION DESIGN DATA

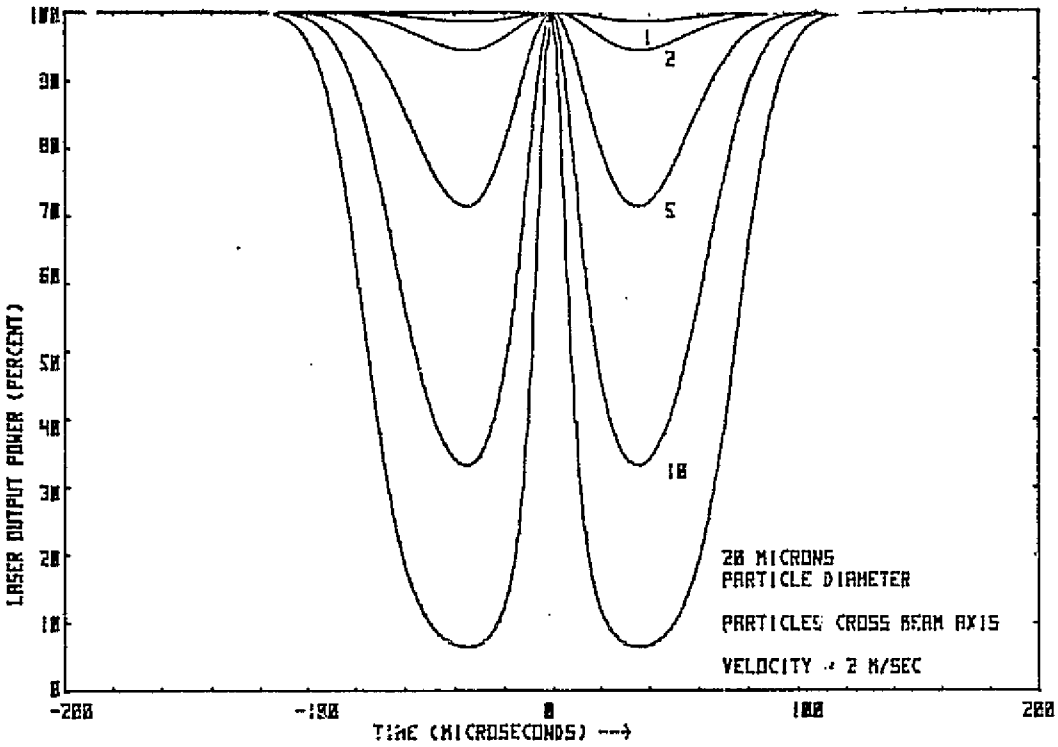

FIGURE 2-9 - LASER EXTINCTION OUTPUT - ON AXIS

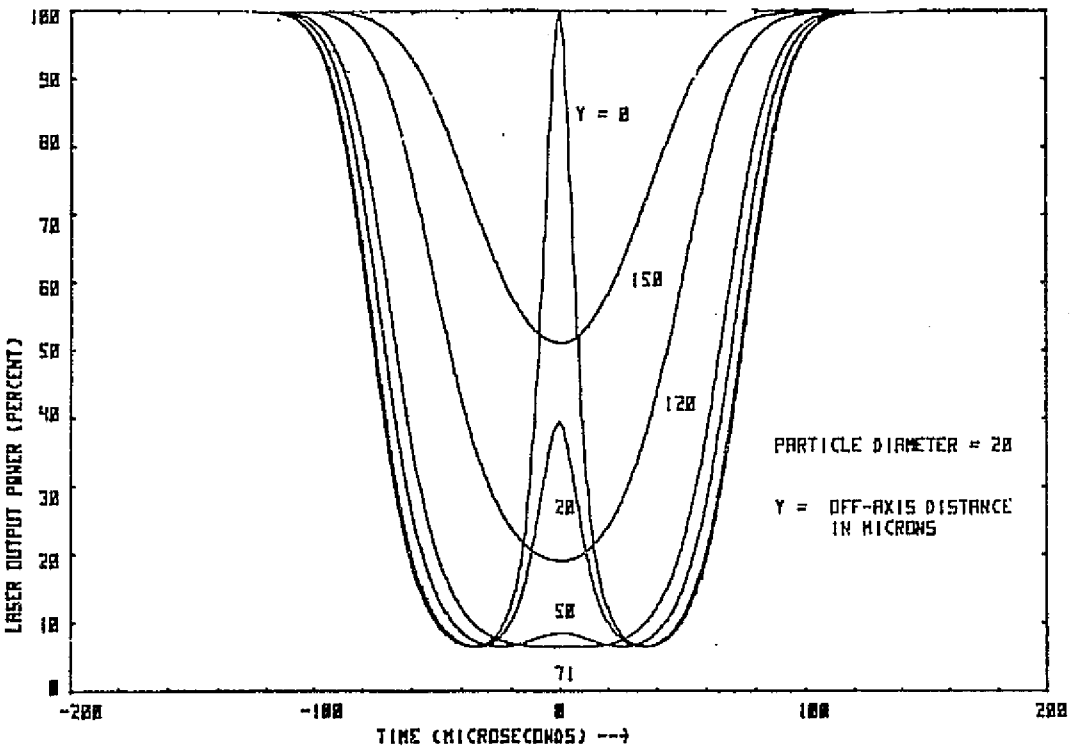

FIGURE 2-10 - LASER EXTINCTION OUTPUT - OFF AXIS

3.0 SYSTEM DESIGN

Details of the optical, mechanical, thermal and electronic design of the Laser Particulate Spectrometer (LPS) are presented in this section. A block diagram of the LPS system is shown in Figure 3-1. The Sensor Head which contains the laser, scattering optics and detectors, is designed to operate in a vacuum chamber. Pulses from the scattering and extinction detectors are processed by the LPS Electronics System to produce standard width pulses for the H-P Model 5401B Multichannel Analyzer (MCA). The H-P Model 9810 Programmable Calculator controls the functions of the MCA and formats the data into particle size and speed spectra suitable for display via x-y plotter.

The principal feature of the optical design was the identification of the parameters of the laser resonant cavity design which would produce the proper mode pattern and intensity level. A concomitant of this procedure is the design of an efficient means for collecting light scattered by the particles.

The key issues involved in the mechanical design were packaging the particle spectrometer in a compact manner, and provisions for hermetically enclosing the laser plasma tube to prevent corona problems involved in reduced pressure operation of the LPS.

Details of the thermal design calculations are presented together with a discussion of the impact of these data on the mechanical design of the LPS system. The LPS electronics system design is detailed together with the considerations involved in interfacing the LPS system to the NASA-furnished 5401B Multichannel Analyzer.

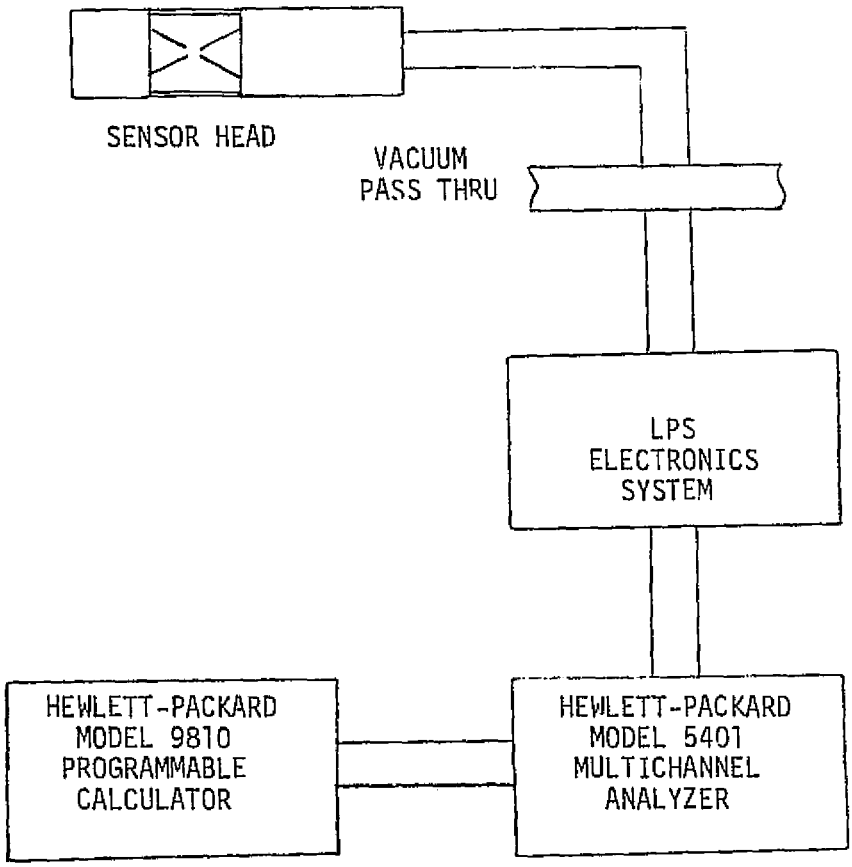

FIGURE 3-1 - LPS SYSTEM BLOCK DIAGRAM

3. OPTICAL DESIGN.

3.1.1 LASER PARAMETERS. In any optical system designed to detect and analyze particle size and velocity distributions, lasers are strong candidates for selection as the primary source of illumination. The laser provides a very intense, well collimated light beam which allows the use of low voltage silicon detectors for scattering measurements, and forms a well defined particle probe volume. Acting as a light amplifier, the laser is a very sensitive system for particle extinction measurements. Several of the laser parameters can be varied to optimize the sensitivity of the system to detect particle fluxes. These include:

- The laser mode pattern
- The laser beam waist diameter
- The intensity of the light incident on the particle.

The effect of varying each of these parameters was evaluated and the results are summarized below.

3.1.2 MODE PATTERN. A laser is capable of operating in one or more of many transverse mode patterns. The most common laser mode is the TEM_{00} or lowest order Gaussian mode. In this mode the laser beam has a peak intensity on the beam axis which then drops off radially as is shown in Figure 3-2. This mode is unsuitable for detecting and sizing particles by scattering or extinction because a large particle passing through the edge of the beam can produce the same size pulse as a smaller particle passing through the center of the beam. For this reason, a higher order mode, the TEM_{01*} degenerate mode, was studied. This mode, shown in Figure 3-3, has a minimum at the center of the pattern, reaches a maximum and then falls off radially from the

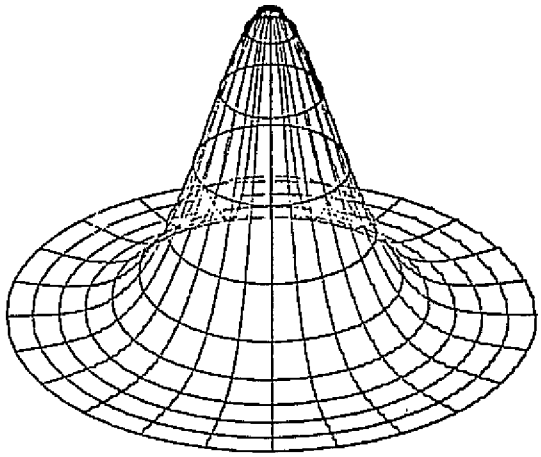

FIGURE 3-2 - TEM_{00} MODE INTENSITY DISTRIBUTION

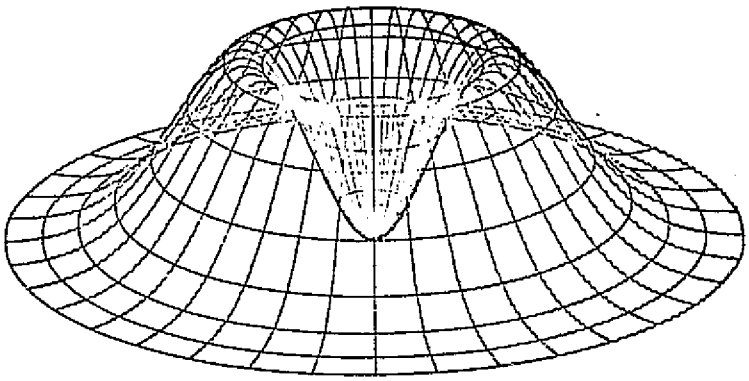

FIGURE 3-3 - TEM_{01*} MODE INTENSITY DISTRIBUTION

axis. A particle traversing the area within the ring of maximum intensity will produce a double pulse the amplitude of which will be dependent on the particle size. Suitable electronic logic can then be devised to detect double pulses and discriminate against single pulses produced when a particle passes through the edge of the beam.

3.1.3 BEAM WAIST DIAMETER. A hemispherical laser resonator cavity consisting of a plane mirror and a spherical mirror forms a laser beam which has a very small intense spot or waist at the plane mirror, and a large, less intense spot at the spherical mirror. For the purposes of small particle detection, the small intense beam is preferred. For a given laser plasma tube, various beam diameters can be obtained by varying the length of the resonant cavity and the focal length of the spherical mirror. This in turn has an effect upon the peak intensity of the mode pattern and the range of particles which can be detected by either scattering or extinction. A detailed analysis of these effects was completed and the results are summarized in Section 3.1.4.

3.1.4 ELECTRO-OPTICAL SYSTEM. In this section the optical design parameters are discussed for a particle spectrometer which will detect, size, and determine the speed of particles from 1.0 to 100μm diameter.

Figure 3-4 shows the major physical parameters of a laser cavity. Given a laser tube of length L_T, with a certain He-Ne gas mixture which determines the gain (g_o), the only variable parameters are: L_o, the overall cavity length; r_s, radius of the spherical mirror; and R_p and R_s, the reflectances of the plane and spherical mirrors respectively. The beam radius at any point within the cavity is given by:

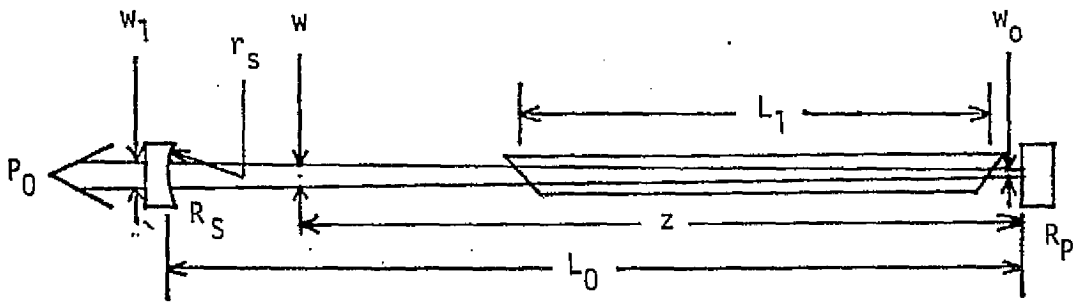

L_o = Cavity Length

L_1 = Plasma Tube Length

R_s = Reflectance of Spherical Mirror

R_p = Reflectance of Plane Mirror

P_o = Output Power

r_s = Radius of Curvature of Spherical Mirror

z = Axial Distance Along Cavity

w_o = Waist Diameter

w_1 = Output Beam Diameter

w = Beam Diameter at Particle Probe Volume

g_o = Unsaturated Gain of Active Medium

FIGURE 3-4 - LASER CAVITY PARAMETERS

$$w(z) = w_o \sqrt{1 + \left(\frac{\lambda z}{\pi w_o^2}\right)^2} \qquad (3.1)$$

where λ is wavelength of light, w_o is the beam waist radius and z is the axial distance from the plane mirror. The waist radius is determined by

$$w_o = \sqrt{\frac{L_o \lambda}{\pi}} \left(\frac{g}{1-g}\right)^{1/4} \qquad (3.2)$$

where $g = 1 - L_o/r_s$.

Figure 3-5 shows the effect on beam radius of varying the radius of the spherical mirror in a cavity of fixed length. Results of an extinction analysis (Figure 2-8) imply that to size particles up to 100μm a beam radius of about 500μm is needed. From Figure 3-5 it is seen that two mirror radii, 60cm and 500cm, give a beam radius of approximately 500μm. A 500cm radius mirror is commonly stocked by laser optics manufacturers and allows operation of the cavity in a region which is not as sensitive to small variations in cavity length as the 60cm mirror. For these reasons a spherical mirror radius of 500cm was initially chosen for the design of the laser cavity. However, it was found that the tapered bore of the Hughes Laser tube would not allow a uniform 500μm beam without excessive diffraction losses so the 60cm mirror was substituted.

The reflectances of readily available commercial laser mirrors are 99.9% for the plane mirror and 97.5% for the spherical mirror; when combined with a plasma tube length of 30cm and an unsaturated gain coefficient of 10%, such mirrors result in a cavity power of 34mW, with a nominal 3mW output beam power level.

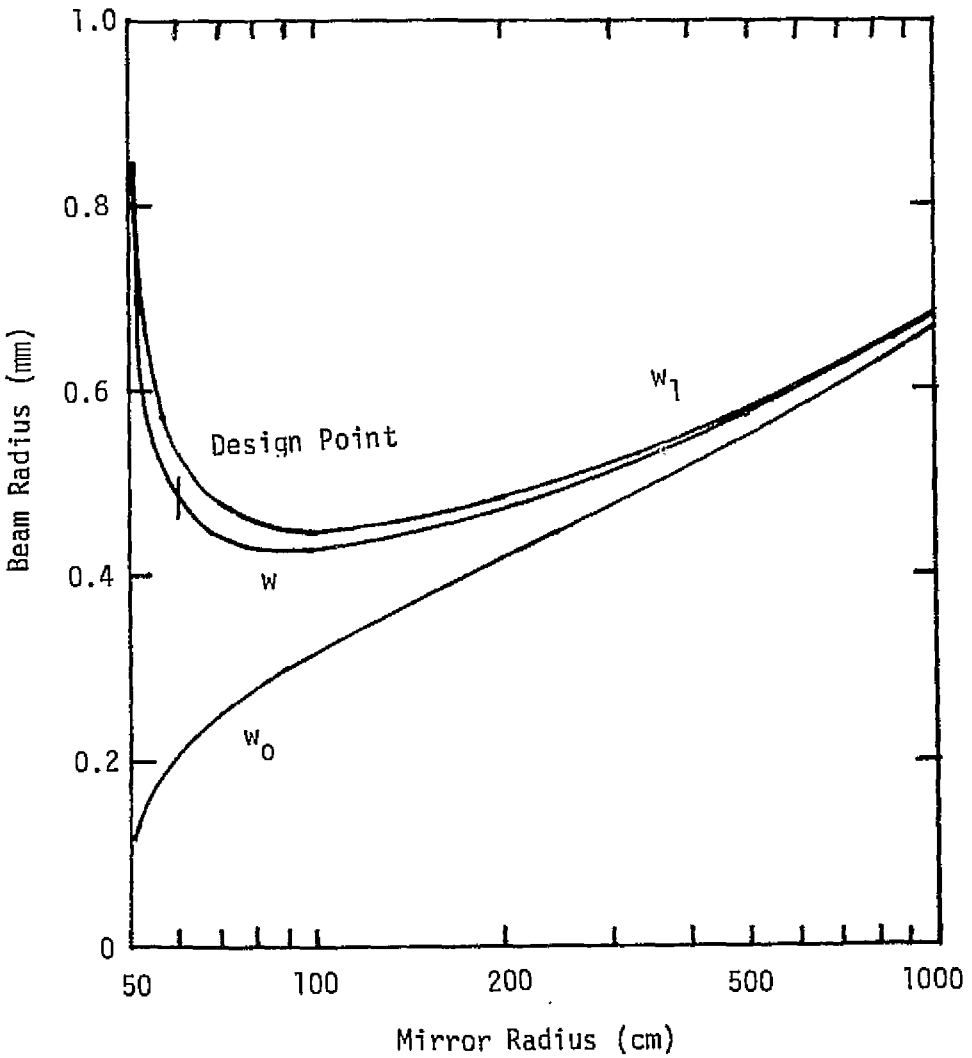

FIGURE 3-5 - LASER CAVITY BEAM DIMENSIONS FOR A 50cm CAVITY

With the laser constrained to oscillate in the TEM_{01*} mode, the intensity of the intracavity beam on the peak isophote is 2.63×10^4 Wm^{-2}, in the absence of a particle. The average irradiance incident on a particle in the beam is a function of both the particle diameter relative to the beam radius and of the degree of extinction of the laser cavity power due to the presence of the particle in the cavity. The effect of the geometrical parameters alone is illustrated in the upper curve in Figure 3-6; above 100μm the average irradiance drops off as the particle diameter approaches the dimensions of the laser beam. The lower curve in Figure 3-6 demonstrates the extinction effect and reveals that the reduction of the intracavity power is the dominant mechanism reducing the irradiance incident on the particle. The laser beam is completely extinguished by particles larger than 275μm diameter. Above 10μm the average irradiance on the particle is such a steep function of particle diameter that an intracavity scattering system would be inappropriate for particles larger than 10μm. It was concluded that the intracavity laser extinction mode should be used for the 10 to 100μm diameter range.

The Mie Scattering program was run again assuming an incident intensity of $2.63 \times 10^4 Wm^{-2}$ and for the scattered power incident on a lens system with annular collection angle between 8.5° and 31°. Figure 3-7 shows the collected power plotted as a function of particle size for four refractive indices. Except for the region between 1.0 and 2.0μm diameter the effects of refractive index are rather small. If particles of known refractive index, e.g. water droplets (n = 1.33), are being analyzed the ambiquities in the 1.0 to 10μm range can be tolerated. However, if a particle flux of unknown refractive index is incident upon the scattering spectrometer, some uncertainity will result in the size determination.

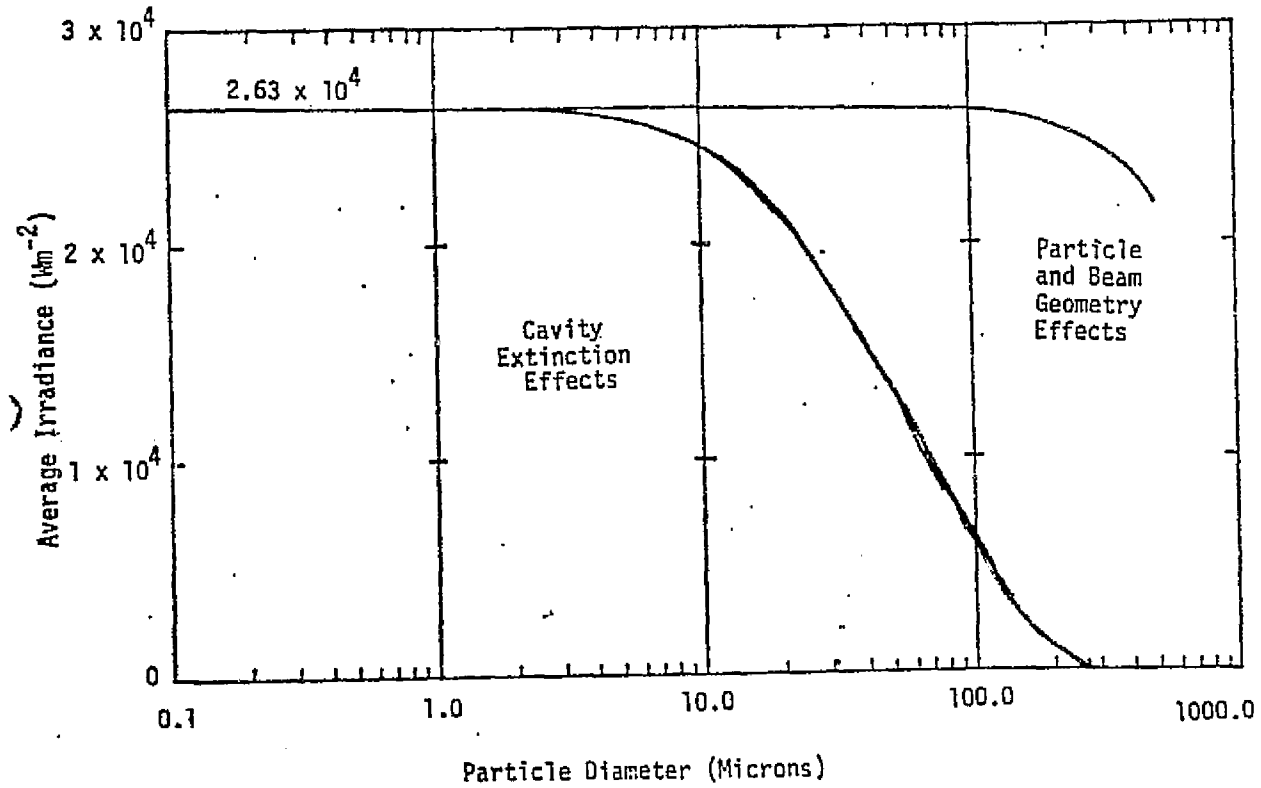

FIGURE 3-6 - AVERAGE IRRADIANCE OF LASER LIGHT INCIDENT ON PARTICLE

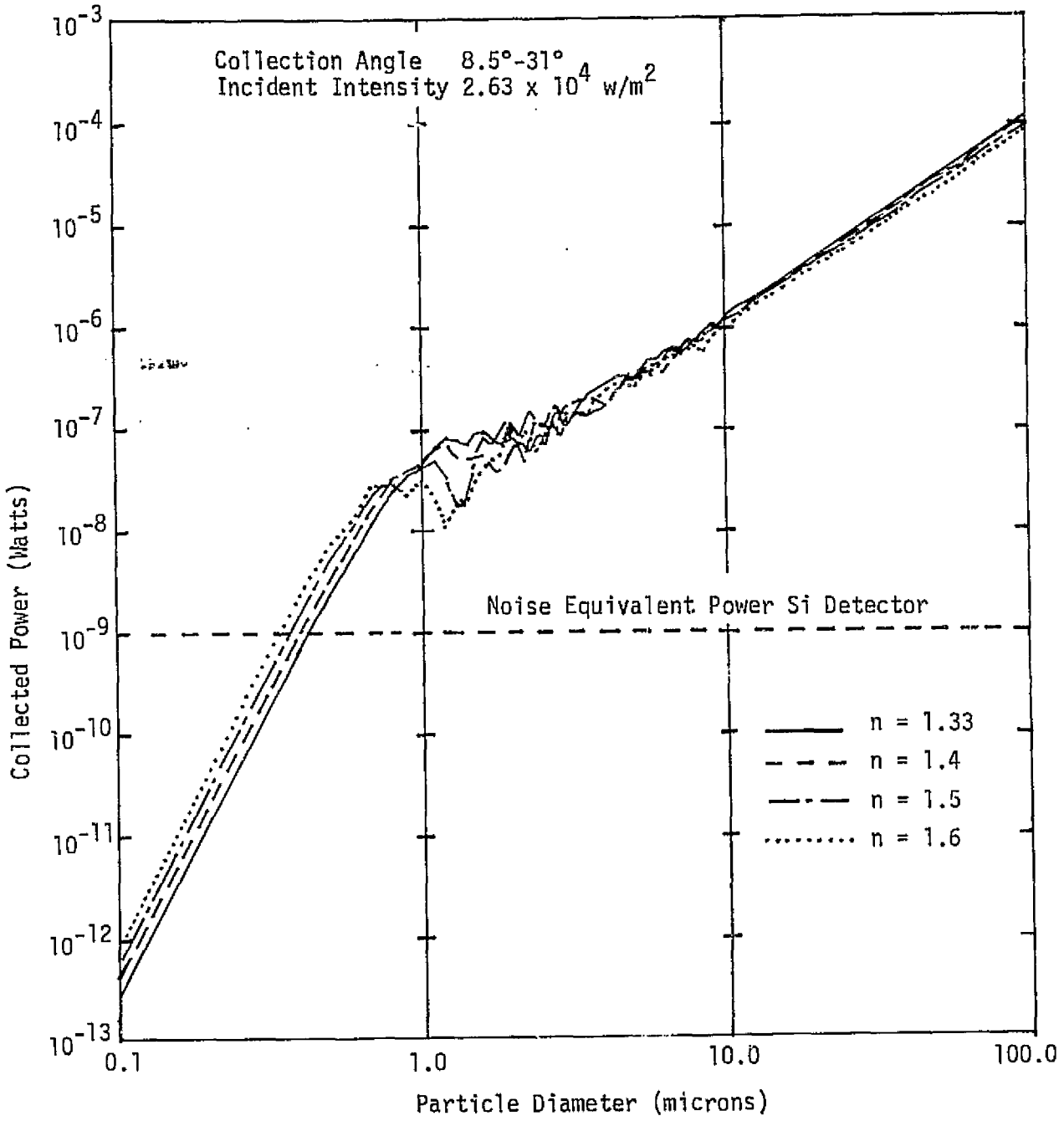

FIGURE 3-7 - COLLECTED SCATTERED POWER (MIE THEORY)

For particle sizes less than 0.6μm diameter, the scattered power drops below the 10^{-9}W noise equivalent power level of the silicon detector.

The theoretical design analysis resulted in a design for the LPS Sensor Head with the following values for the key parameters:

- Lasing medium - helium-neon gas
- overall cavity length - 50cm
- spherical mirror radius - 60cm
- mirror reflectances - 99.9% and 97.5%
- output power (extra-cavity) - 3mW nominal
- cavity power (intra-cavity) - 34mW
- peak incident intensity (intra-cavity) - $2.63 \times 10^{4} Wm^{-2}$
- beam parameters:

  w_o = 272μm

  w_1 = 520μm

  w = 477μm at z = 45cm
- scattered power (intra-cavity)

  0.1μm ~ 10^{-12} watts

  1.0μm ~ 2×10^{-8} watts

  10.0μm ~ 10^{-6} watts
- extinction power (normal output power = 3.0mW)

  10.0μm ~ 2.8mW

  100μm ~ 0.6 W

  275μm ~ 0.00 (laser oscillation ceases)
- $TEM_{01}*$ mode

Figure 3-8 shows a schematic representation of the Sensor Head optical design. The highly collimated laser output beam passes through holes in lenses L1 and L2 and is directed onto the extinction detector by the small plane mirrors M1 and M2. The probe volume, defined by two conical aluminum baffles is coincident with the focus of lens L1. Particles which traverse the probe volume scatter light into lens L1, which functions as a collimator. Lens L2 re-focuses the scattered light onto the scattering detector. The laser plasma tube and the plane laser resonator mirror are located within an hermetic enclosure to prevent corona discharge problems during vacuum chamber pump-down. The laser beam passes through a compensating Brewster window attached to the hermetic enclosure. The second Brewster window removes the translational offset produced by the first window to maintain the laser beam congruent with the mechanical axis of the Sensor Head.

3.2 SENSOR HEAD MECHANICAL DESIGN. The majority of the mechanical design effort in this program was concentrated on the Sensor Head. A number of mechanical design considerations were determined by the selection of the Hughes Model 3184H He-Ne laser. This laser consists of a glass plasma tube which is mounted in a 1.75 inch OD x 12.5 inch long aluminum tube using a flexible potting compound. This laser was selected after reviewing the range of commercially-available models, because the aluminum tube could be conveniently clamped to a heat sink with small probability of mechanical stress on the glass plasma tube and because the cavity mirrors could be detached from the metal tube for intracavity work.

The dimensions of the laser and the system requirements defined in the thermal analysis of Section 3.3 established the size of the laser hermetic enclosure and, to a large extent, the overall size of the entire Sensor Head.

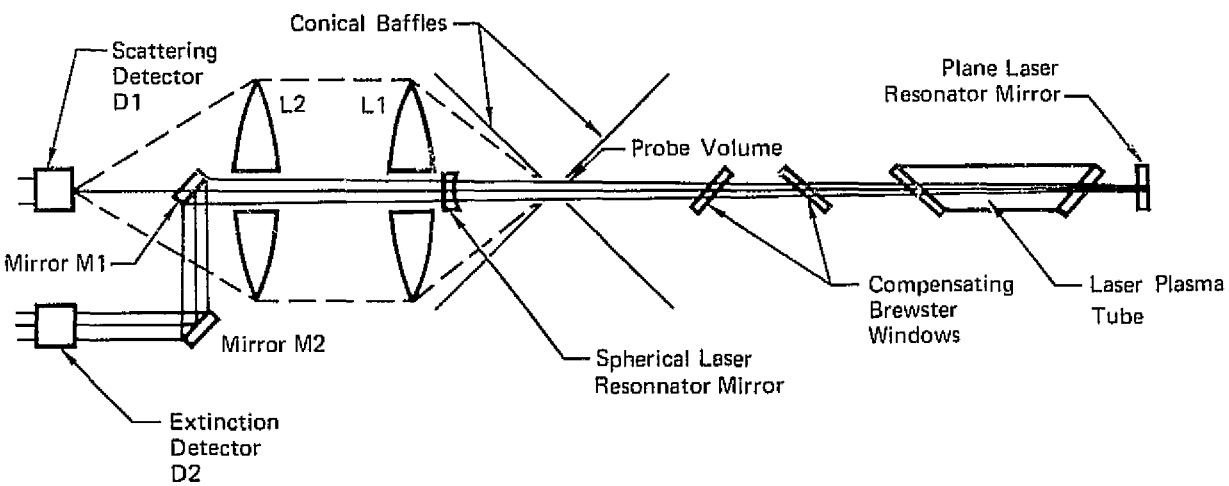

FIGURE 3-8 - SENSOR HEAD DETAILS

A basic cylindrical geometry was selected for the Sensor Head for simple design and ease of fabrication.

The assembly drawing for the LPS is shown in Figure 3-9. The design of the mounting structure for the laser plasma tube incorporates the dual requirements of providing a heat sink for the plasma tube and a high thermal conductance path to the cylindrical shell. The section cut A-A of Figure 3-9 shows the heat sink with a semi-cylindrical machined groove into which the laser is clamped. Deep penetration heliarc welds were used to attach the heat sink to the 17.5cm OD cylindrical shell. Two rectangular fins, integral to the heat sink, were included to increase the radiating surface area of the Sensor Head hermetic enclosure. The result of this design was to produce a combined heat sink-radiator assembly which permits efficient rejection of waste heat produced by the laser plasma tube and the laser high voltage power supply.

The ends of the cylindrical shell are closed by aluminum end plates which mate with internal flanges. The rear plate carries a flat window through which the laser beam exits allowing a view of the resonant mode of the laser cavity during alignment of the LPS system. A valve is provided on the rear end plate for pumping and backfilling the hermetic enclosure with dry gas (nitrogen or helium).

The front end plate carries a double Brewster window, which is located inside the laser resonant cavity. The dual window is required to compensate for lateral displacements of the laser beam caused by a single window. In this way the laser beam remains congruent with the principle symmetry axis of the Sensor Head.

Two conical aluminum baffles are employed to define the length of the LPS probe volume (~1mm). Proper spacing between the tips of the baffles is maintained by four low thermal expansion Invar rods which carry the scattering

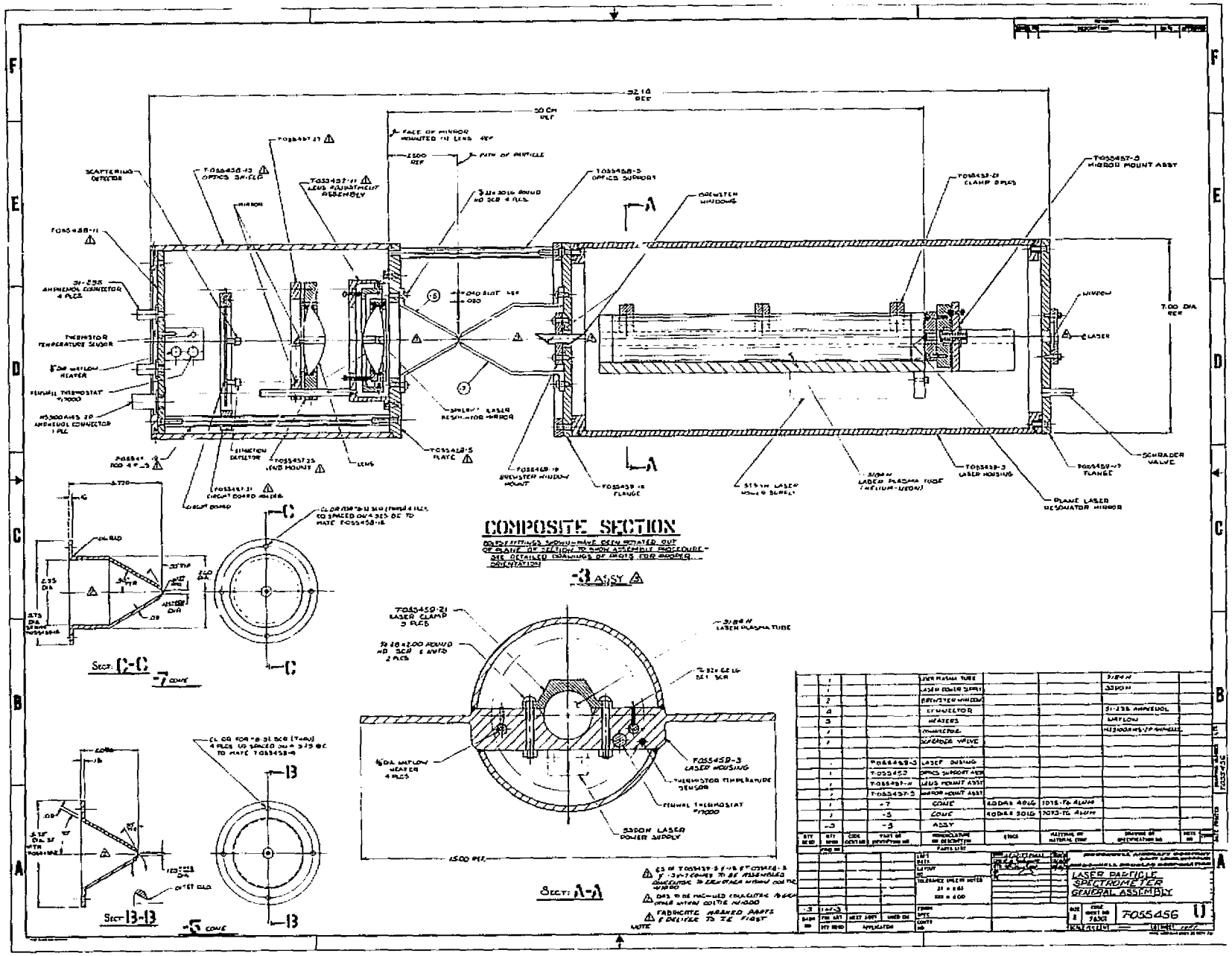

FIGURE 3- - SENSOR HEAD ENGINEERING ASSEMBLY DRAWING

optics and detector assembly. This assembly is located in a light-tight non-hermetic enclosure. The two lenses which comprise the scattering optics are carried on adjustable mounts supported on three alignment rods. Four additional rods carry the circuit card on which the two photodiode detectors and preamplifiers are mounted and the end plate on which the electrical connectors and heater are carried. The weight of the Sensor Head is approximately 84 kgm.

3.3 LASER THERMAL ANALYSIS. The laser head in the particle spectrometer is contained within a gas-filled hermetic enclosure. This has the effect of minimizing helium loss from the laser plasma tube, minimizing corona discharge problems, and promoting heat transfer via gaseous convection. However, the heat generated by the laser plasma tube and power supply (within the hermetic enclosure) still had to be dissipated from the entire package. This was complicated by the restraints which prohibited the use of liquid or gas cooling and by the portability required of the Sensor Head. In addition the Sensor Head had to be capable of operating in vacuum within the LN_2-cooled shroud of a space simulation chamber.

Effects of laser overheating and undercooling include degradation of the Brewster window seals, due to expansion or contraction and decomposition of the epoxy used to bind the windows to the tube, and perturbations of the resonant cavity due to unequal expansion of the component parts. Thus, it is necessary to minimize temperature variations while the particle spectrometer is in operation.

A simple computer model was used to analyze the thermal performance of the LPS Sensor Head. For steady-state radiative heat transfer between the exterior surfaces of the Sensor Head and the cold shroud, the equilibrium

optics and detector assembly. This assembly is located in a light-tight non-hermetic enclosure. The two lenses which comprise the scattering optics are carried on adjustable mounts supported on three alignment rods. Four additional rods carry the circuit card on which the two photodiode detectors and preamplifiers are mounted and the end plate on which the electrical connectors and heater are carried. The weight of the Sensor Head is approximately 84 kgm.

3.3 LASER THERMAL ANALYSIS. The laser head in the particle spectrometer is contained within a gas-filled hermetic enclosure. This has the effect of minimizing helium loss from the laser plasma tube, minimizing corona discharge problems, and promoting heat transfer via gaseous convection. However, the heat generated by the laser plasma tube and power supply (within the hermetic enclosure) still had to be dissipated from the entire package. This was complicated by the restraints which prohibited the use of liquid or gas cooling and by the portability required of the Sensor Head. In addition the Sensor Head had to be capable of operating in vacuum within the LN_2-cooled shroud of a space simulation chamber.

Effects of laser overheating and undercooling include degradation of the Brewster window seals, due to expansion or contraction and decomposition of the epoxy used to bind the windows to the tube, and perturbations of the resonant cavity due to unequal expansion of the component parts. Thus, it is necessary to minimize temperature variations while the particle spectrometer is in operation.

A simple computer model was used to analyze the thermal performance of the LPS Sensor Head. For steady-state radiative heat transfer between the exterior surfaces of the Sensor Head and the cold shroud, the equilibrium

temperature of the Sensor Head surface, Tsh, is given by

$$T_{sh} = \left[\frac{Q_{int}}{\epsilon_{sh}\sigma A_{sh}} + T_{cs}^4\right]^{1/4} \qquad (3.1)$$

where

Q_{int} = internal heat generation (W)

ϵ_{sh} = thermal emittance of the external surface of the Sensor Head

σ = Boltzmann constant

A_{sh} = surface area of the Sensor Head

T_{cs} = cold shroud temperature.

The available design parameters are the emittance σ_{sh} and the surface A_{sh} of the Sensor Head.

The basic thermal design criterion, to maintain the temperature of the laser plasma tube within allowable limits (253 to 323°K) for shroud temperatures from 77 to 300°K, establishes the required surface area, A_{sh}, for a given emittance, ϵ_{sh}.

The worst case condition as far as laser overheating is concerned occurs when the laser is operating in a high vacuum environment with the cold shroud at room temperature (~300°K). This condition establishes the minimum surface area, A_{sh}, required to maintain T_{sh} below 323°K, the maximum laser temperature. To insure that the temperature of the laser plasma tube does not differ significantly from the surface temperature, T_{sh}, the plasma tube is attached to a massive aluminum heat sink which is in good thermal contact with the exterior surface of the Sensor Head enclosure (see Figure 3-9).

Likewise, the worst case condition for laser undercooling occurs for the 77°K cold shroud. This condition establishes the minimum internal heat generation, Q_{int}, required to maintain the laser temperature above 253°K.

Figure 3-10 shows the Sensor Head temperatures T_{sh} as a function of cold shroud temperature for a number of coatings. The solid curves were calculated for internal heat generation of 30W corresponding to the nominal heat dissipation of the laser. The dashed curves refer to 100W of internal heat generation. The surface area A_{sh} is $0.4m^2$ for these calculations.

All of the coatings listed above are seen to provide satisfactory thermal performance for cold shroud temperatures from 77 to 300°K with $A_{sh} = 0.4m^2$. The black anodize coating was selected for the Sensor Head because of its durability. Two thick fins, integral with the laser heat sink; were included in the design to give a total surface area (fin plus cylinder) for the laser hermetic enclosure of approximately $0.42m^2$.

3.4 LPS ELECTRONICS SYSTEM DESIGN. Figure 3-11 shows a block diagram of the LPS Electronics System. Three separate functions are provided by this system, viz, supplying power to the laser, control of the Sensor Head temperature, and interfacing between the detectors and the H-P 5401B MCA. Several of the components of the electronics system are packaged in Nuclear Instrumentation Modules (NIM) blank modules.

3.4.1 LPS DETECTORS AND PREAMPLIFIERS. Silicon photodiode detectors are employed to measure the scattering and extinction signals. The preamplifiers convert detector current pulses into voltage outputs and drive these pulses through the LPS Cable System.

3.4.2 CABLES AND VACUUM FEEDTHROUGH. Each detector/preamplifier combination has a line driver which converts the current pulses from the detectors into voltage pulses and provide sufficient current drive capability to power 150 feet twinax cables. One hundred feet of cable is located inside the

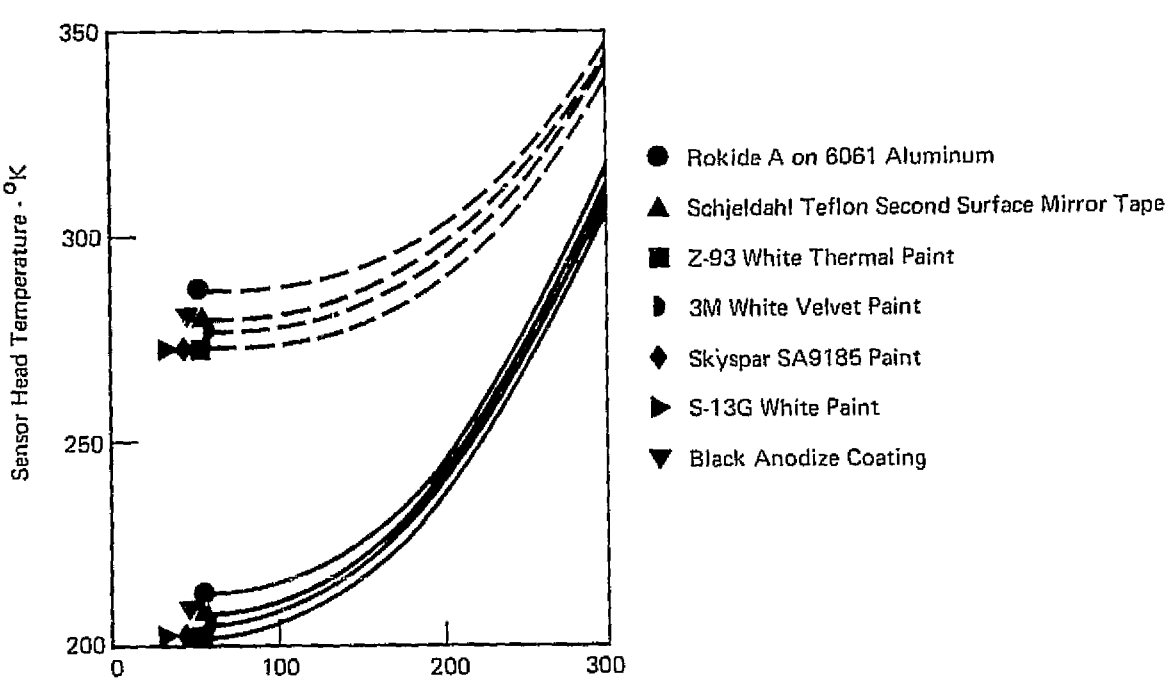

FIGURE 3-10 - SENSOR HEAD RADIATIVE EQUILIBRIUM TEMPERATURE

vacuum chamber while the remaining 50 feet is located outside. The vacuum feedthrough consists of hermetic electrical connectors mounted on a plate attached to a port of the vacuum chamber.

3.4.3 CHANNEL SELECT MODULE. This unit contains line receiver amplifiers which provide high rejection of common-mode signals which under some circumstances may accompany the detector output pulses. Additional circuitry monitors the pulses in the two channels, selects pulses from either the scattering of the extinction channel and passes them to the Signal Conditioning Module (SCM).

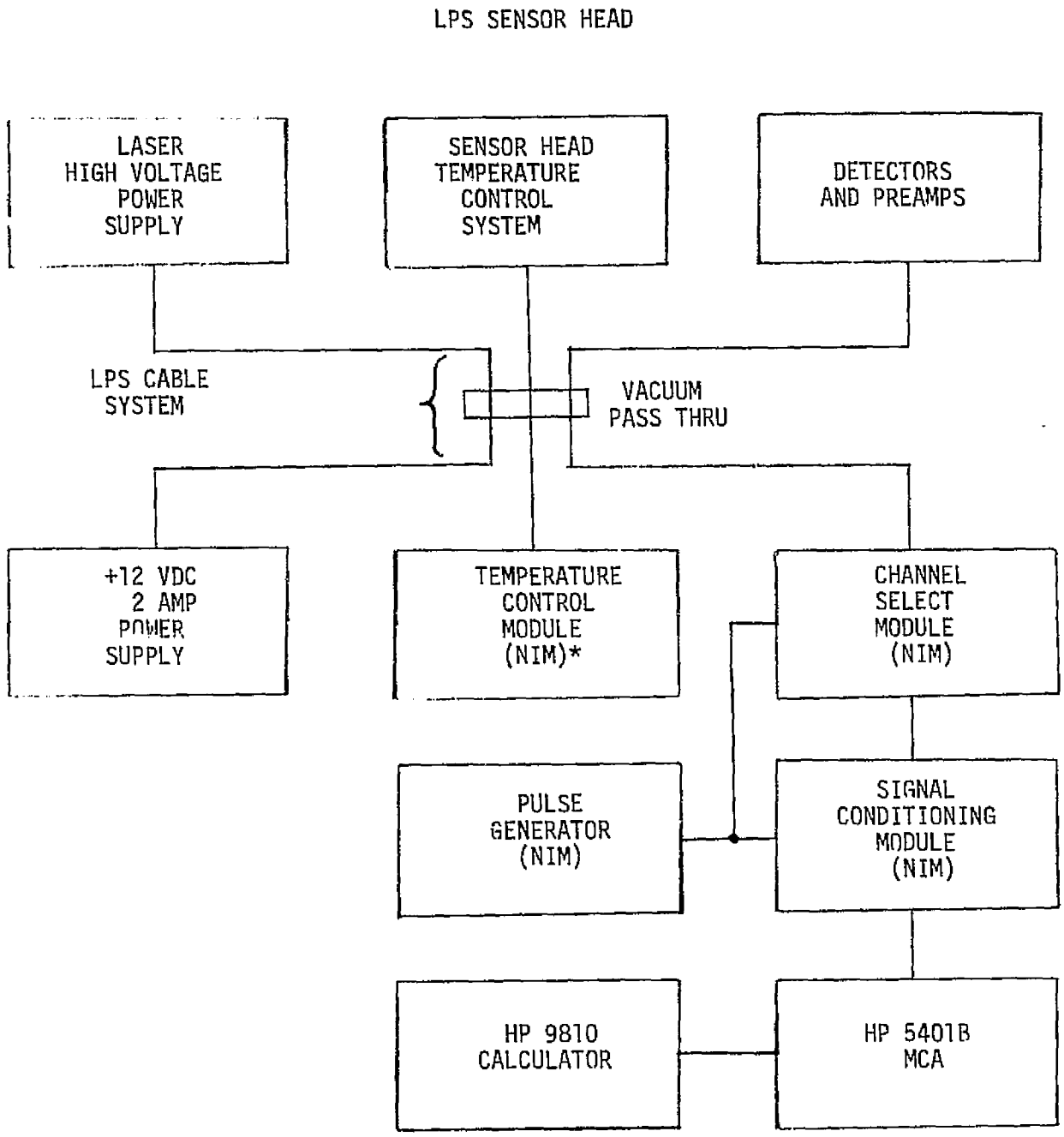

*Nuclear Instrumentation Module Package

FIGURE 3-11 LPS ELECTRONICS SYSTEM BLOCK DIAGRAM

3.4.4 SIGNAL CONDITIONING MODULE. This unit contains the circuitry required to produce pulses proportional in height to the particulate size and transit time across the laser beam. The Double Pulse Discriminator (DPD) circuit accepts double pulses generated by particles which pass through the axis of the laser beam and rejects single pulses produced by particles which make grazing encounters with the laser. The Time-of-Flight (TOF) circuit measures the duration of the double pulses to yield the particulate transit time through the laser beam. The Dead-Time-Counter (DTC) circuit provides the means for resetting the LPS Electronics System when a single pulse is encountered. The Reset/Memory Routing/Clock circuit generates reset pulses, 2MHz clock pulses for the TOF circuit, and the memory routing pulses required by the H-P 5401B MCA for operation in the "external memory routing" mode.

3.4.5 PHA/PROGRAMMABLE CALCULATOR SYSTEM. The Electronics System of the Laser Particulate Spectrometer is designed to utilize the capabilities of a Hewlett Packard 5401B Multichannel Analyzer - 9810 Programmable Calculator System for pulse height analysis of the spectrometer size and speed data, for displaying size and speed spectra via CRT monitors and x-y plotter and for storing spectral data on a digital magnetic tape cassette. The LPS supplies size and speed data in a continuous fashion to the 5401B which operates as a pulse height analyzer (PHA). The functions of the PHA (accumulation of spectra, display, and storage of data) can be controlled either manually via the PHA front panel controls or automatically under program control via the 9810 Programmable Calculator. The PHA/Programmable Calculator System has no direct control of the functions of the LPS which operates continuously once the laser and the LPS Electronics Systems are powered. A description and operating procedure for the specialized software developed to control this

system is contained in Volume II.

3.4.6 TEMPERATURE CONTROL SYSTEM. The operating temperatures of the laser, detectors preamplifiers and line drivers contained in the Sensor Head are controlled by the Temperature Control System (TCS) which consists of the Temperature Control Module (TCM), thermistor sensors, thermostats and cartridge heaters. The operating temperature range of the laser (253°K to 323°K) must not be exceeded for any environment in which the Sensor Head is operated. Under laboratory conditions (i.e. room temperature, one atmosphere pressure) the normal equilibrium temperature for the laser is approximately 317°K. When the Sensor Head is operated in a vacuum chamber with a 300°K cold shroud, the radiative heat transfer between the Sensor Head and the cold shroud will yield an equilibrium temperature near 315°K with the normal laser dissipation of about 30W. This equilibrium temperature depends on the thermal emittance of the anodized aluminum exterior ($\varepsilon_{th} = 0.82$) and the surface area ($\sim 0.42 m^2$) of the Sensor Head as well as on the internal heat generation due to the laser. The Sensor Head cannot be operated in a solar simulator beam as a severe overtemperature condition will result. If it is necessary to so operate the Sensor Head, either a shading screen can be used to prevent direct irradiation of the Sensor Head by the beam, or a solar reflecting paint such as Z-93 or 3M White Velvet Paint can be applied to the Sensor Head. These paints are easily removed by solvents or mechanical abrasion if it is desired to return to the black anodize condition.

When operating the Sensor Head with reduced cold shroud temperatures (down to 77°K), the TCS functions to maintain the temperature of the Sensor Head between 280°K and 300°K. A digital temperature indicator is provided in the TCS module to monitor two thermistors, one located in the aluminum

heat sink near the laser and the other near the detectors and preamplifiers.

3.4.7 PULSE GENERATOR (PG). Various types of pulse outputs useful for checking and aligning the LPS Electronics Aystem are available from the Pulse Generator, Figure 3-12. The waveform of Figure 3-12a is used as a simulated scattering doublet which is input to the CS module. Similarily, the EXTIN-OUT waveform from the PG module, Figure 3-12b, is a simulated extinction doublet for aligning the CS module extinction channel. Two synchronizing waveforms, Figures 3-12c and d, are available at the PG module, SYNC-OUT and $\overline{\text{SYNC}}$-OUT.

The amplitude of the SCAT-OUT waveform can be adjusted via the SCAT-AMP

(a) SCATTERING CHANNEL TEST WAVEFORM

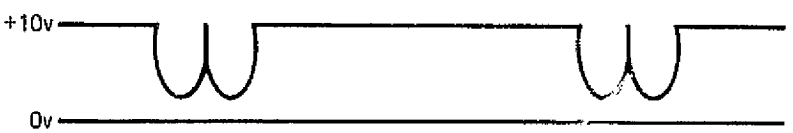

(b) EXTINCTION CHANNEL TEST WAVEFORM

(c) SYNC OUT TEST WAVEFORM

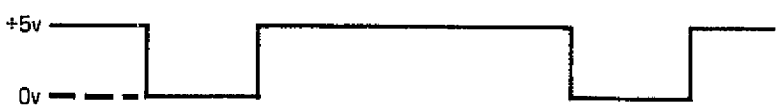

(d) $\overline{\text{SYNC}}$ OUT TEST WAVEFORM

FIGURE 3-12 - PULSE GENERATOR TEST WAVEFORMS

potentiometer, while the amplitude of the EXTIN-OUT doublet is adjusted by means of the EXTIN-AMP pot. In addition, the positive DC level of the EXTIN-OUT waveform can be varied by the EXTIN-DC LEVEL pot. A PHASE adjustment is provided to produce symmetrical doublets and to eliminate the effects of switching transients on the various PG outputs.

A SINGLET-DOUBLET toggle switch allows the selection of either single or double pulses at the SCAT-OUT and EXTIN-OUT receptacles. This function is particularly useful for checking the performance of the double pulse discriminator (DPD). The DPD when functioning properly, will process the doublets and completely reject the singlets.

4.0 LPS SYSTEM DEVELOPMENT

Fabrication and assembly details for the LPS System are discussed in this section. A description of the LPS System operation is given together with a discussion of the method of calibrating the outputs of the LPS in terms of particulate size and transit time spectra.

4.1 COMPONENT FABRICATION. Detailed engineering drawings of the LPS Sensor Head components are shown in Figure 3-9 and Figures 4-1 thru 4-4. Component fabrication was accomplished in the machine shops of McDonnell Douglas Corporation. The majority of the components were fabricated from 6061-T6 aluminum alloy. The exceptions are the four support rods, connecting the laser hermetic enclosure and the detector housing, which were fabricated from Invar rod stock, a low thermal expansion steel alloy. The aluminum components were cleaned and then anodized with a sulfuric acid anodize treatment.

The components comprising the laser hermetic enclosure were heli-arc welded. Helium leak detection techniques were employed to verify the vacuum-tight condition of the hermetic enclosure.

4.2 ASSEMBLED HARDWARE. Figure 4-5 shows the assembled LPS Sensor Head mounted on a gimballed support which provides ±45° adjustment in altitude and 360° in azimuth. The front panel of the LPS Electronics System is shown in Figure 4-6. Standard NIM Bin hardware was used to house the circuit cards. Figure 4-7 shows the LPS data acquisition system consisting of the LPS Electronics System, H-P 5401B Multichannel Analyzer, H-P 9801 Programmable Calculator and H-P Digital Magnetic Cassette Tape Unit. Not shown in this figure is the H-P 9862A X-Y Plotter which is normally used to produce hard-copy of the size and speed spectra.

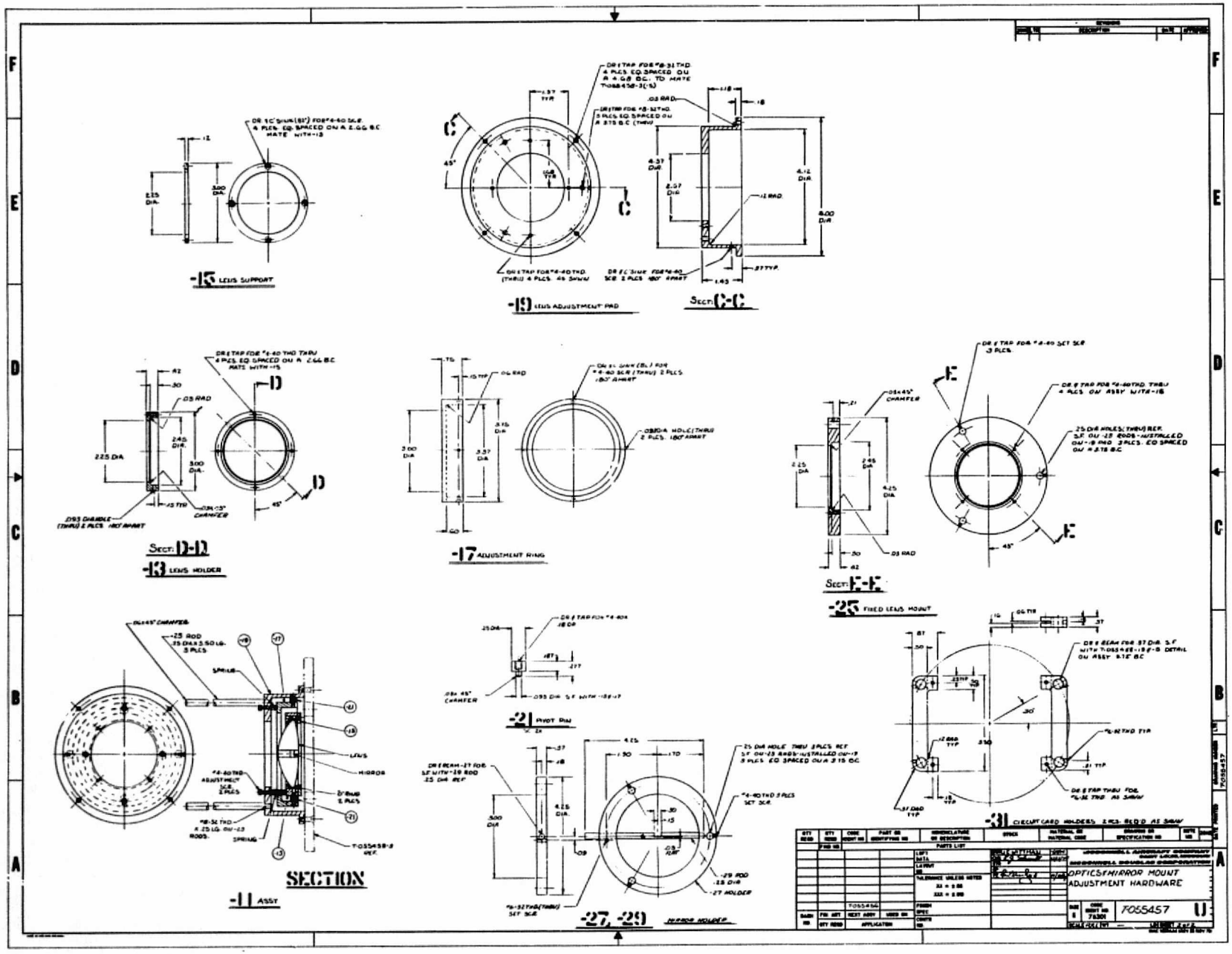

FIGURE 4-1 - OPTICS AND MIRROR MOUNT ADJUSTMENT HARDWARE

ORIGINAL PAGE IS
OF POOR QUALITY

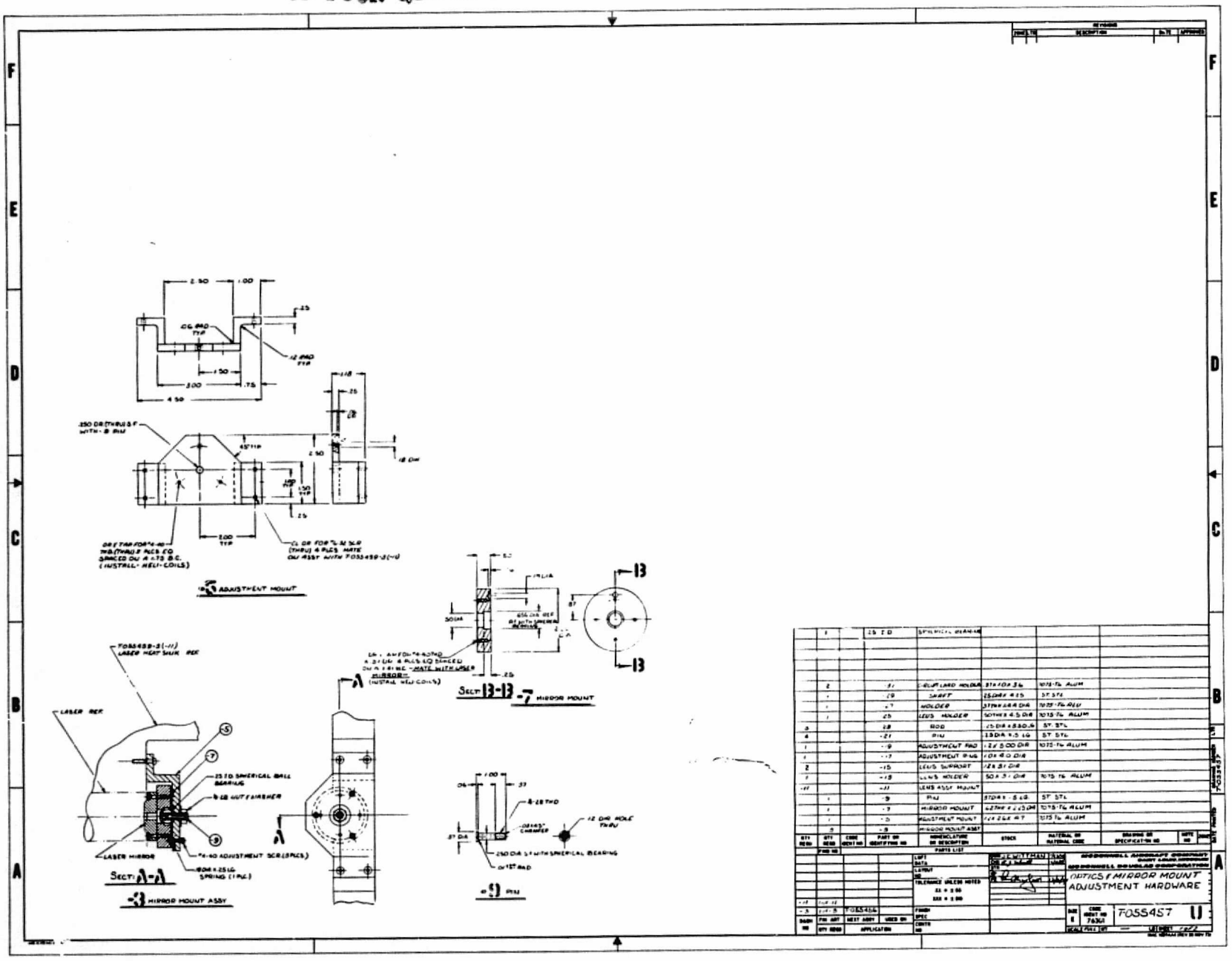

FIGURE 4-2 - OPTICS AND MIRROR MOUNT ADJUSTMENT HARDWARE - CONTINUED

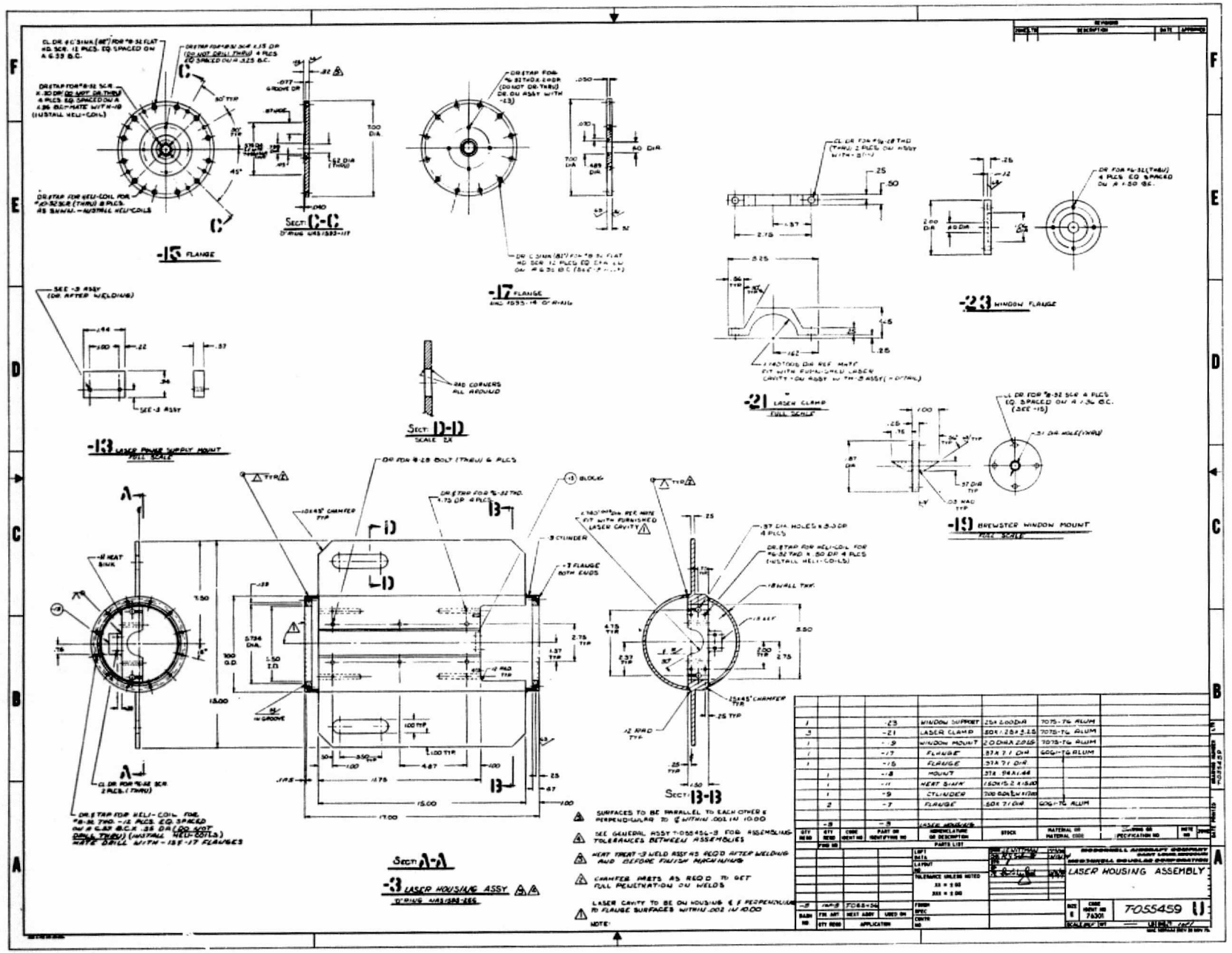

FIGURE 4-3 - LASER HOUSING ASSEMBLY

ORIGINAL PAGE IS
OF POOR QUALITY

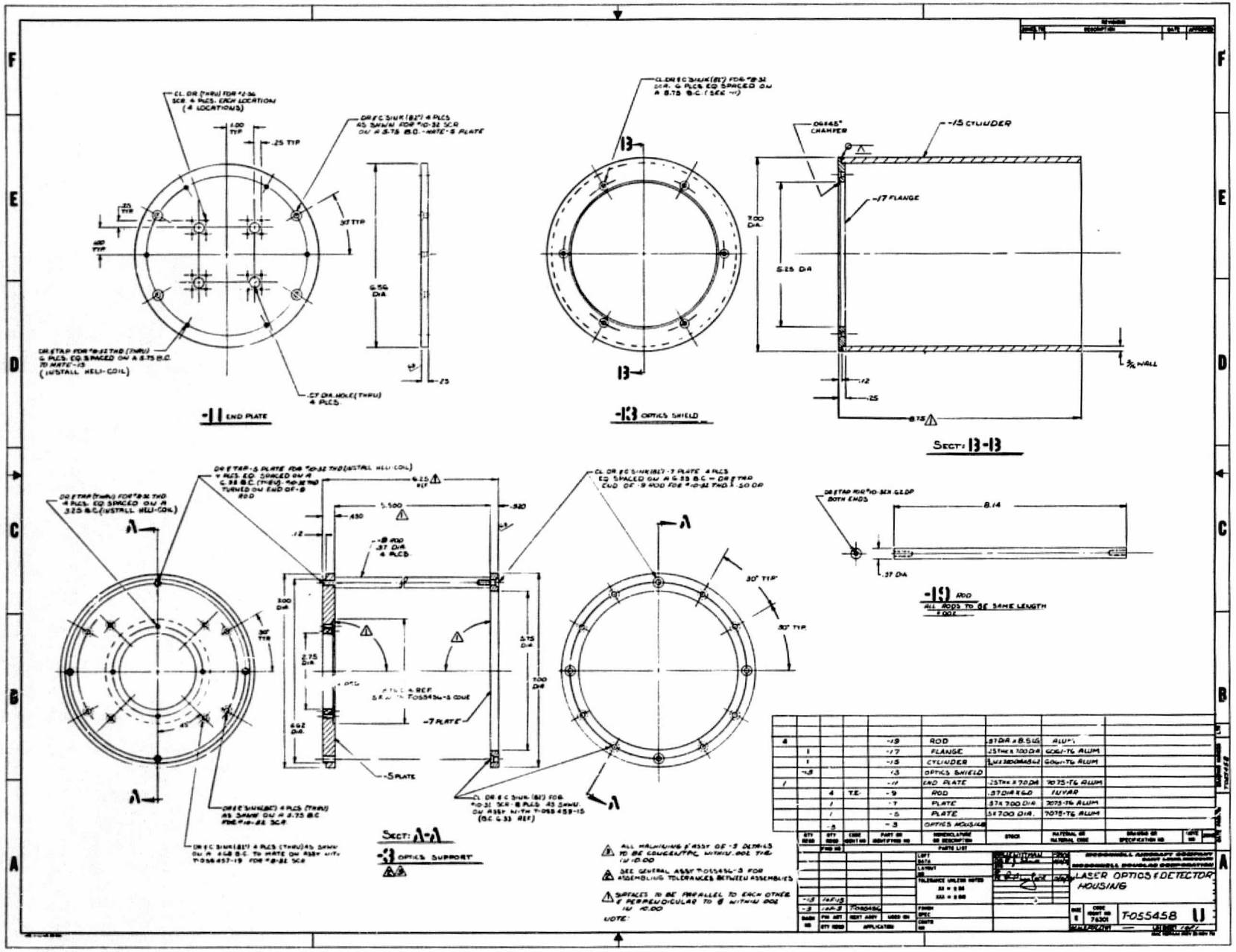

FIGURE 4-4 - LASER OPTICS AND DETECTOR HOUSING

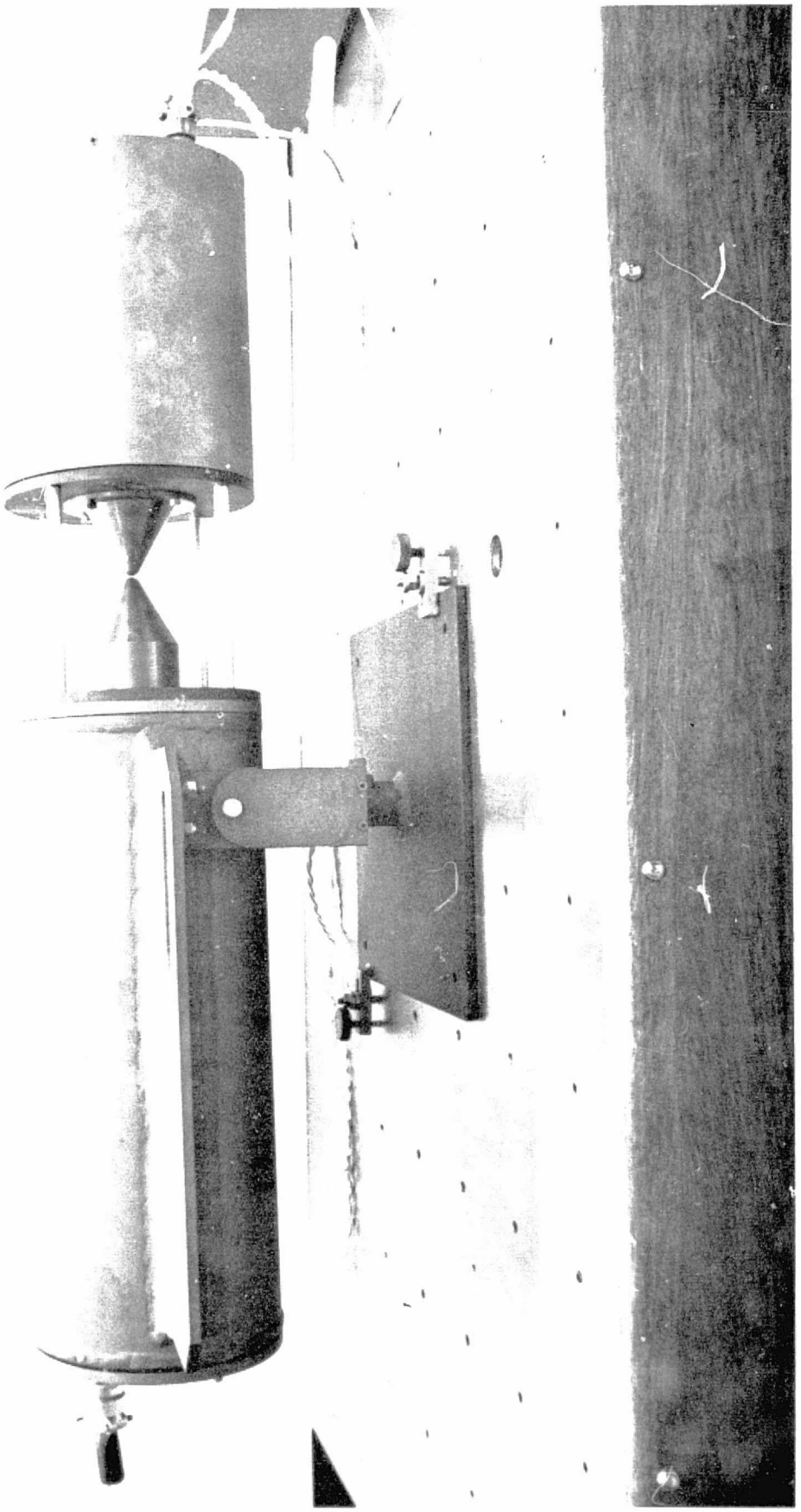

FIGURE 4-5 - LPS SENSOR HEAD

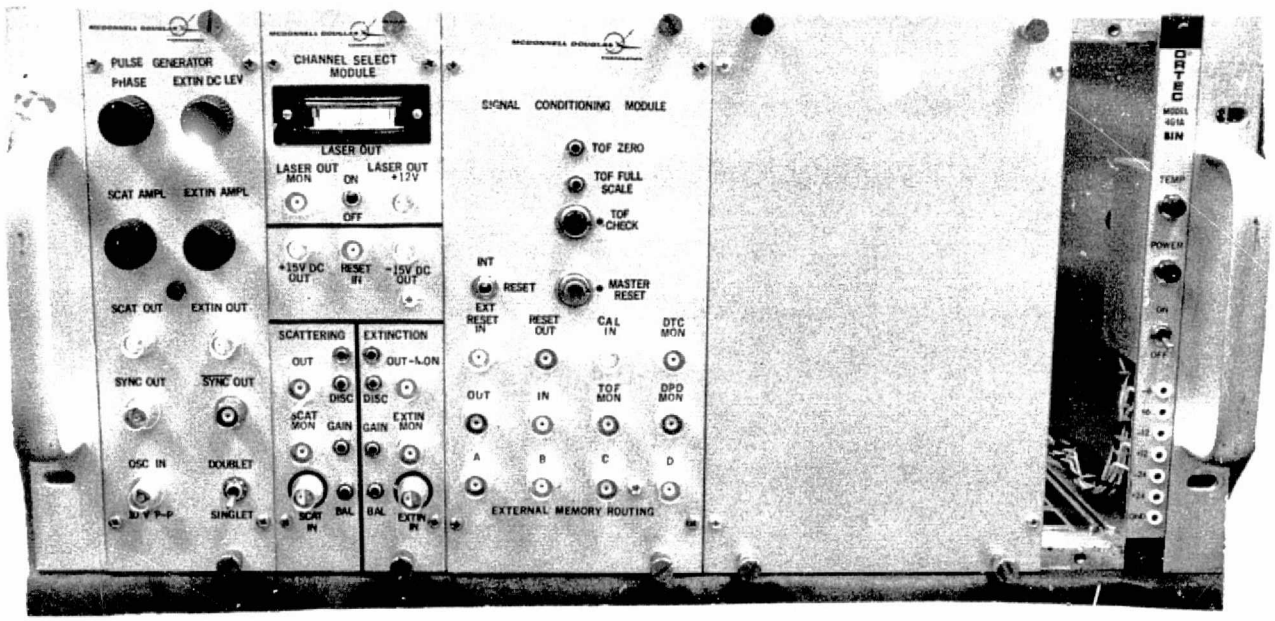

FIGURE 4-6 - LPS ELECTRONICS SYSTEM

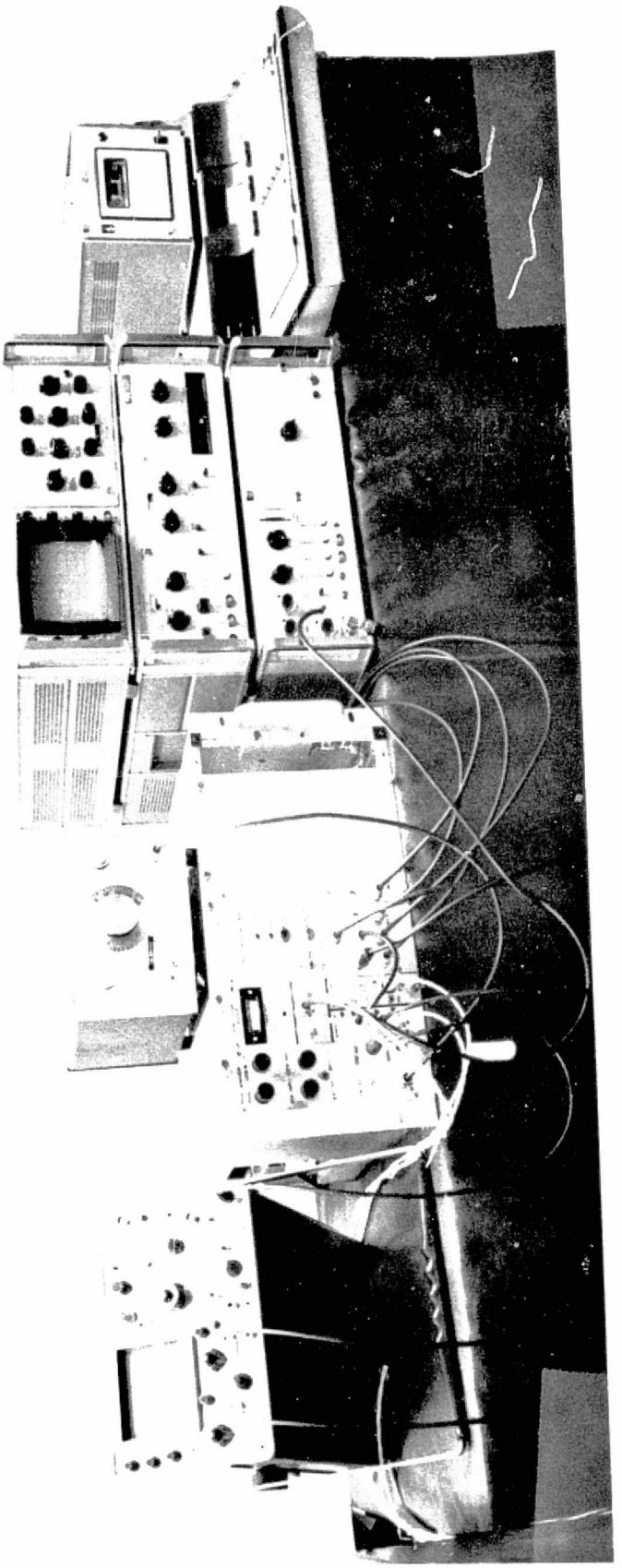

FIGURE 4-7 - LPS DATA ACQUISITION SYSTEM

4.3 LPS SYSTEM OPERATION. Details of the LPS System operation procedure are contained in Volume II.

4.4 SYSTEM CALIBRATION. Calibration of the LPS System is conceptually straightforward. Particles of known size are introduced into the probe volume and the resulting PHA spectra are recorded. The electronic gains of the two channels are then adjusted to obtain the desired calibration curve relating particle size and/or speed to LPS output voltage levels. The major problems in the calibration are, first, obtaining the particles with known size and, secondly, generating a sufficiently high flux of these particles for introduction into the LPS probe volume. A substantial portion of this program was directed towards developing means of calibrating the LPS. After investigating electrostatic and ultrasonic means of generating calibration particles and after attempting to employ a cascade impactor, the methods described in the following two sections allowed a calibration to be accomplished.

4.4.1 SCATTERING CHANNEL SIZE CALIBRATION. The scattering channel calibration was accomplished by introducing polystyrene latex particles of known size into the probe volume. A Royco Particle Generator was used to produce a stream of dry latex particles from a liquid suspension. A specially designed nebulizer produced an aerosol consisting of small water droplets and latex particles. This aerosol is passed through a drying column which evaporated the water particles and left an exiting stream of dry latex particles.

The scattering channel calibration of Figures 4-8 thru 4-11 were obtained using the calculator programs designed especially for the LPS system. The size spectra shown in this section were produced by the calculator-controlled X-Y plotter under program control. The PHA 0 to 10 volts input range was adjusted to span 256 PHA channels, such that the spectra shown in this section

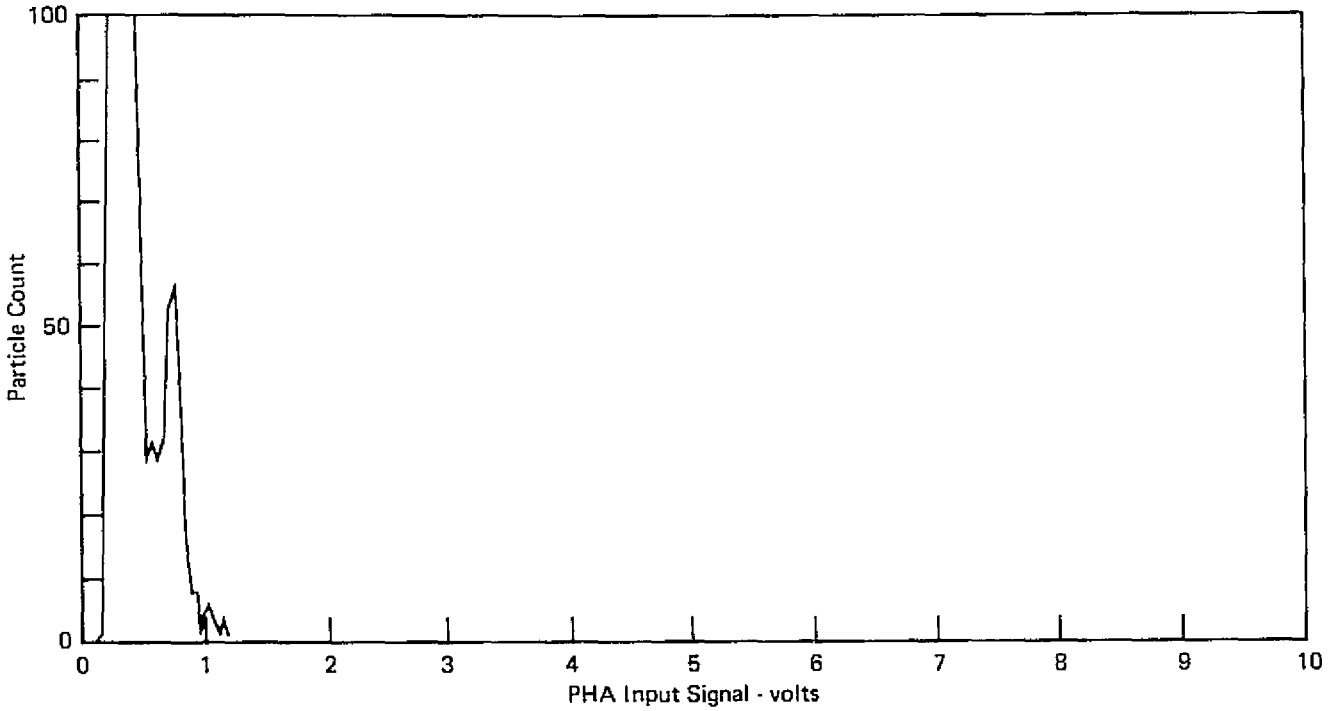

FIGURE 4-8– SCATTERING CHANNEL SIZE SPECTRUM
0.81 MICRON DIAMETER LATEX PARTICLES

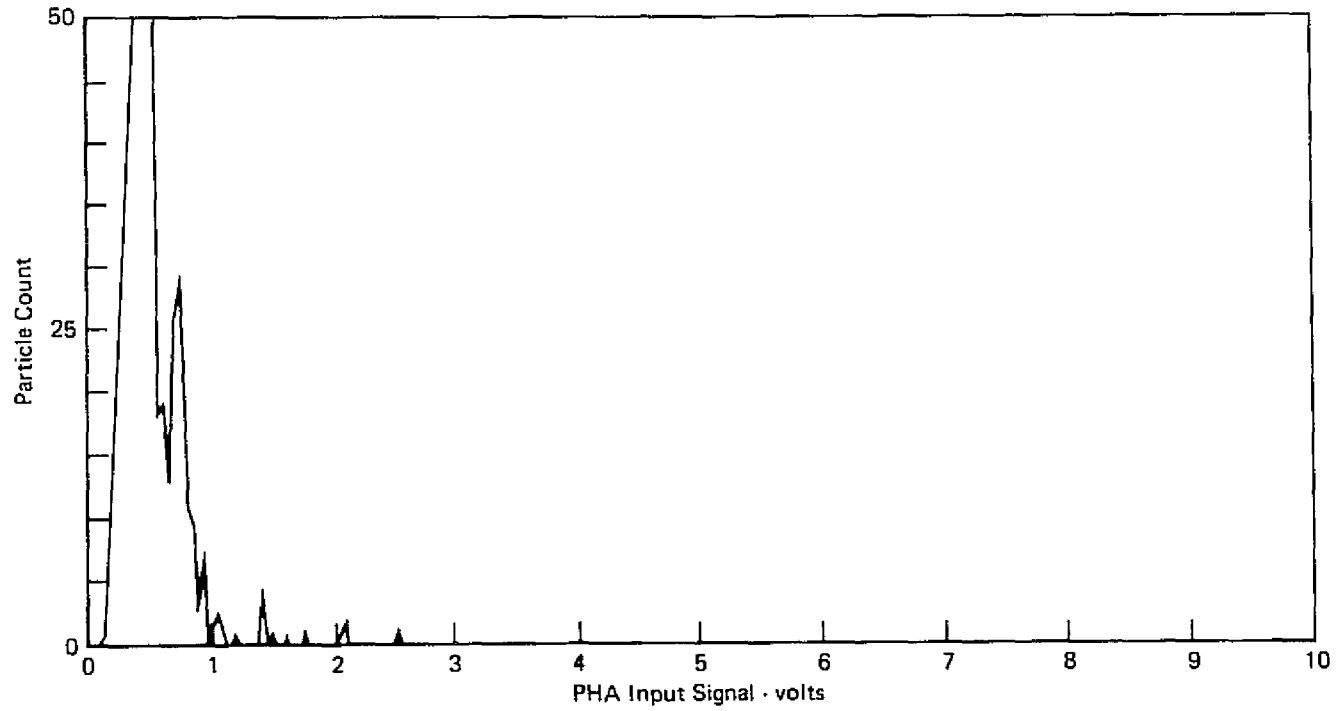

FIGURE 4-9 – SCATTERING CHANNEL SIZE SPECTRUM
1.17 MICRON DIAMETER LATEX PARTICLES

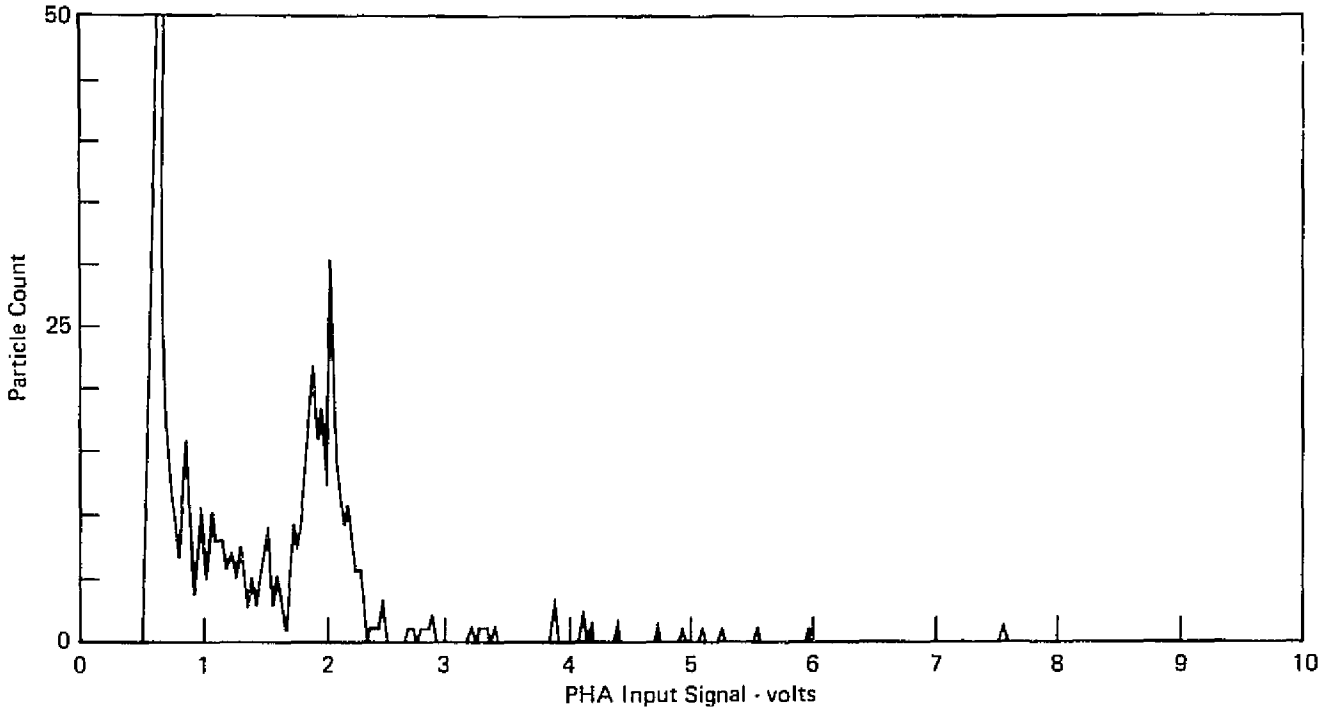

FIGURE 4-10–SCATTERING CHANNEL SIZE SPECTRUM
2.68 MICRON DIAMETER LATEX PARTICLES

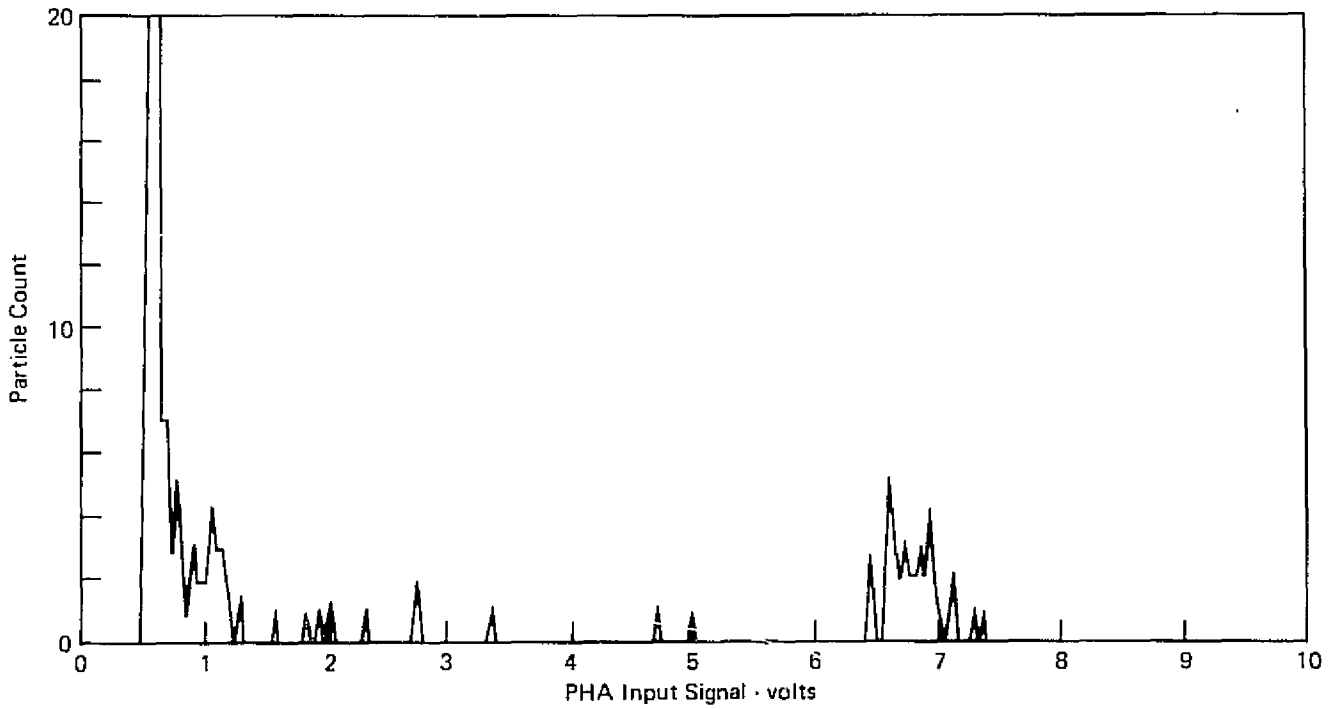

FIGURE 4-11– SCATTERING CHANNEL SIZE SPECTRUM
3.49 MICRON DIAMETER LATEX PARTICLES

are plots of the particle count in each of these 256 channels.

The large peak at approximately 0.5V appearing in each scattering channel size spectrum is due to large numbers of small incompletely evaporated water aerosol droplets. This was verified by operating the Royco generator with distilled water minus the latex particles. It should be noted that the random noise due to the electronics circuits is approximately 50mV. This voise level increases by a factor of nearly four when the laser is operating due to scattering from the numerous small (<0.5μ diameter) dust particles which pass through the laser beam in a normal laboratory environment. The threshold level of the scattering discrimination was set to approximately 0.3V to eliminate this background noise from the system. This sharp cutoff of the low voltage side of the large peak is due to the action of the discriminator.

Attempts were made to generate latex particle fluxes of size greater than 3.49μ diameter. The practicable upper limit for the Royco generator, however, is approximately 5μ diameter.

The scattering channel calibration data is summarized in Figure 4-12. The two curves are derived from Mie scattering theory applied to the inter-cavity laser design used in the LPS System. The refractive index 1.5 curve applies to latex particles while the n = 1.33 curve typifies water particles. These curves, which were scaled such that a 10μm diameter particle corresponds to a 10V pulse from the LPS, represent theoretical calibration curves for the LPS scattering channel.

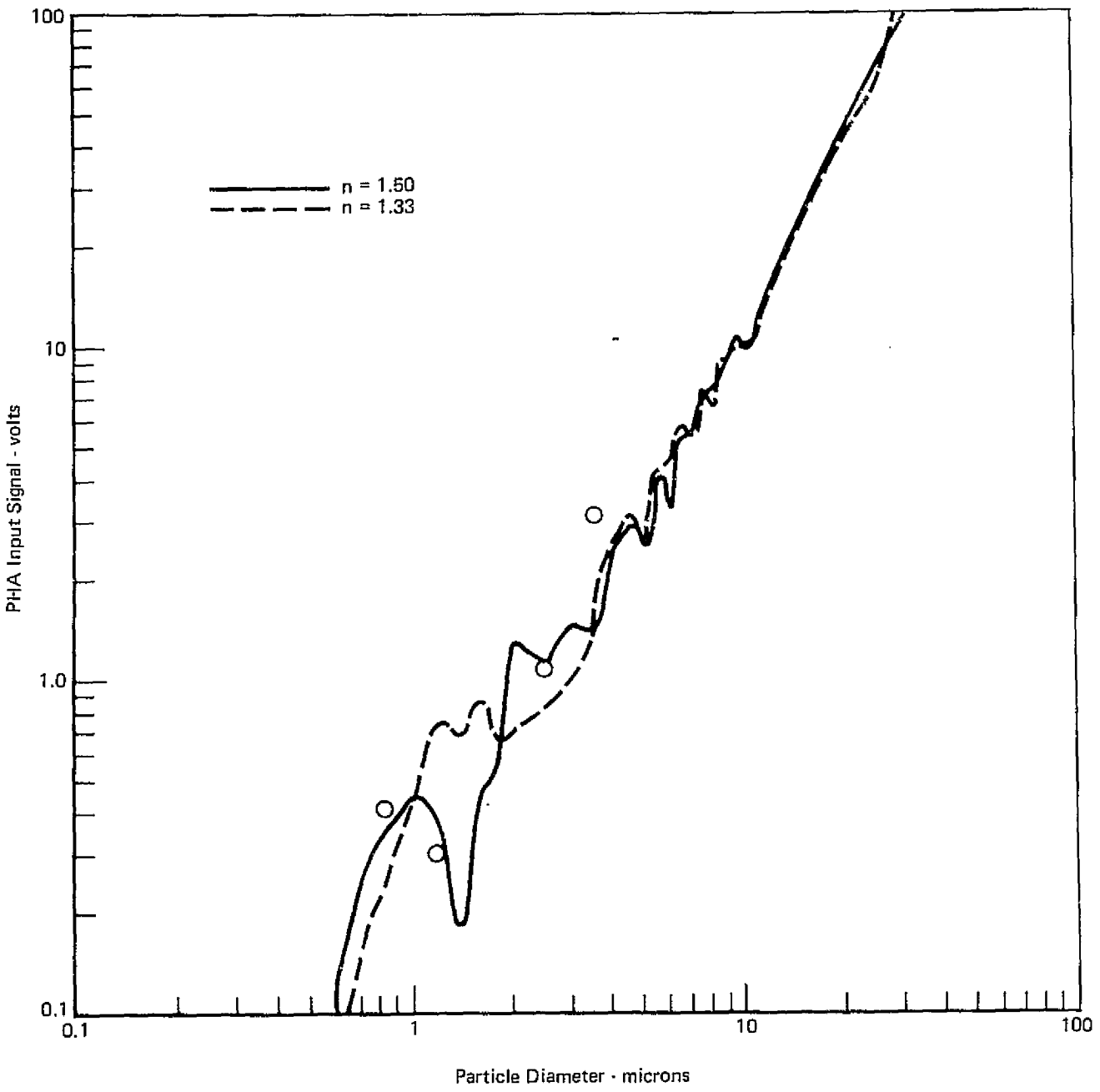

FIGURE 4-12– SCATTERING CHANNEL CALIBRATION CURVE

calibration procedure is to adjust the gain appropriately to obtain the desired calibration curve.

4.4.2 EXTINCTION CHANNEL SIZE CALIBRATION. The extinction channel calibration was obtained using spherical glass beads obtained from the Cataphote Corp., Jackson, Mississippi, and the dry particle generator shown in Figure 4-13. Two sets of data are shown in Figures 4-14 thru 4-20. The large peak in these spectra centered at approximately 0.5V is due to multiple coincidence effects which reduce the laser beam intensity sufficiently to cause the extinction channel noise level to rise above the discriminator threshold level. The coincidence problem is caused by random "bursts" of particles, unavoidable in this type of particle generator, which momentarily cause large fluctuations in the intensity of the laser beam.

Several of the spectra (Figures 4-16 and Figures 4-20) show the effects of two sizes of particles simultaneously interacting with the laser beam to produce two distinct peaks. This was unintentional and later investigation showed that the second peak was due to glass beads which were trapped inside the conical baffles which define one probe volume dimension. These particles apparently were convected by the air stream from the dry particle generator and interacted with the laser beam inside the baffles to produce their characteristic extinction pulses.

The spectrum produced in the Houston calibration for 44-55μm diameter glass beads, Figure 4-18, shows a much wider peak than was obtained in the previous calibration run with these particles, Figure 4-15. It is believed that the wider peak is due to traces of moisture in the flask of the Dry Particle Generator which caused agglomeration of the glass beads. Clusters consisting of two and three adhering glass beads tumbling through the laser beam are expected to produce broadened peaks, such as that of Figure 4-18.

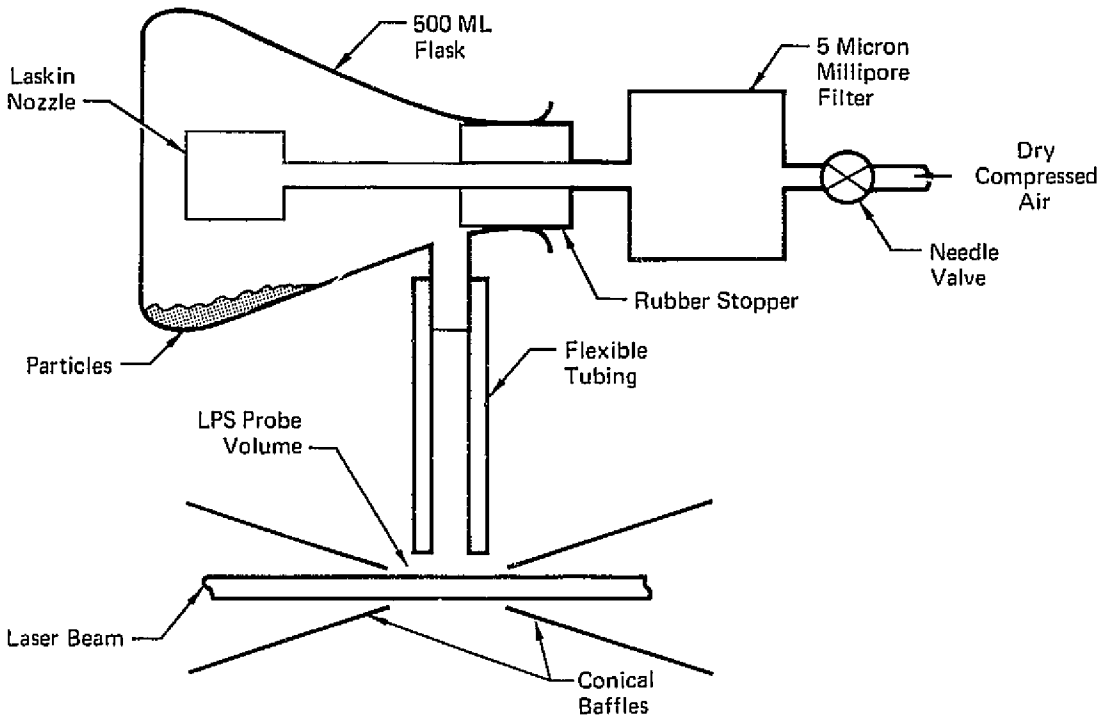

FIGURE 4-13- DRY PARTICLE GENERATOR

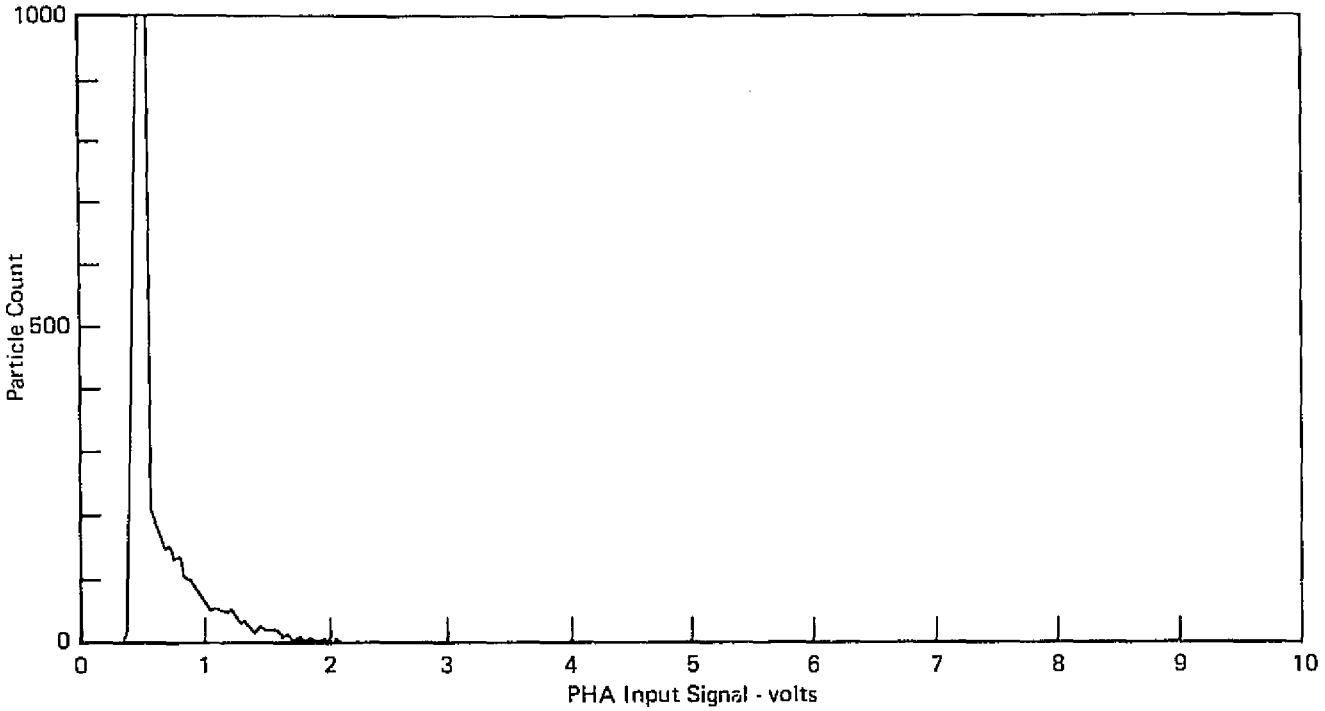

FIGURE 4-14 – EXTINCTION CHANNEL SIZE SPECTRUM
15-37 MICRON DIAMETER GLASS BEADS

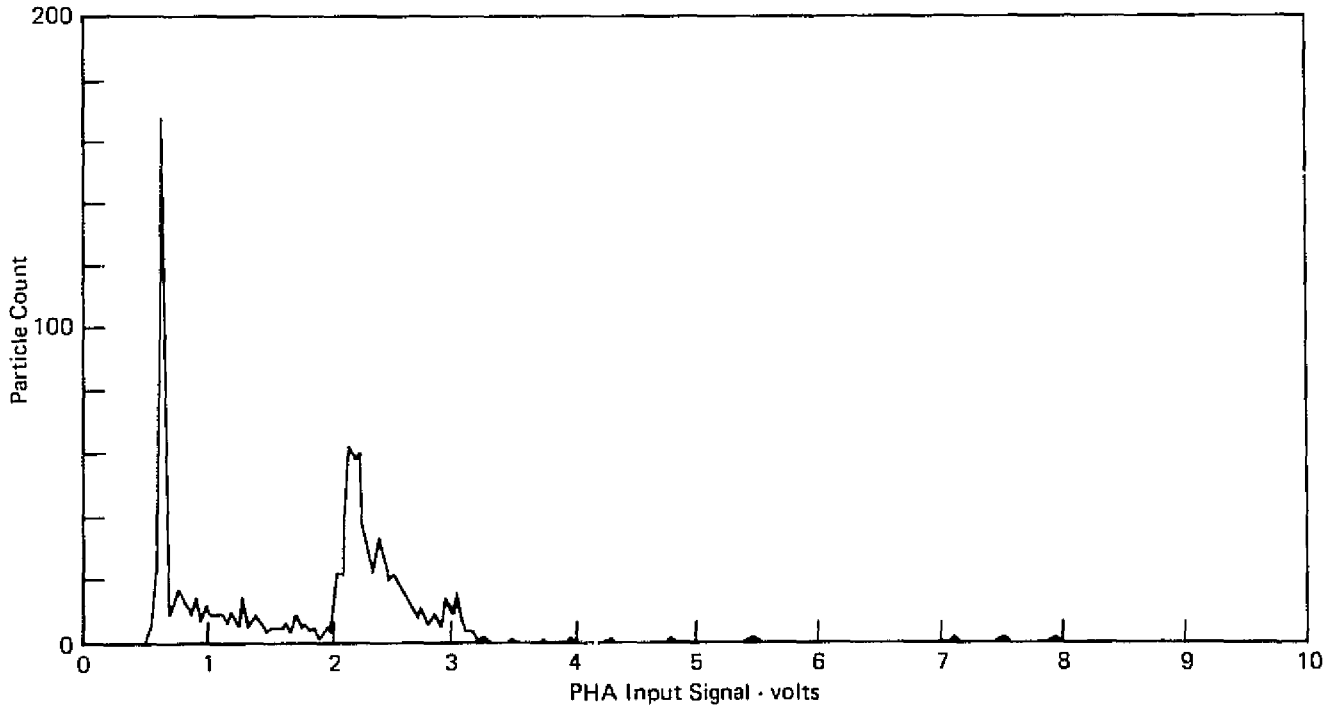

FIGURE 4-15 – EXTINCTION CHANNEL SIZE SPECTRUM
44-55 MICRON DIAMETER GLASS BEADS

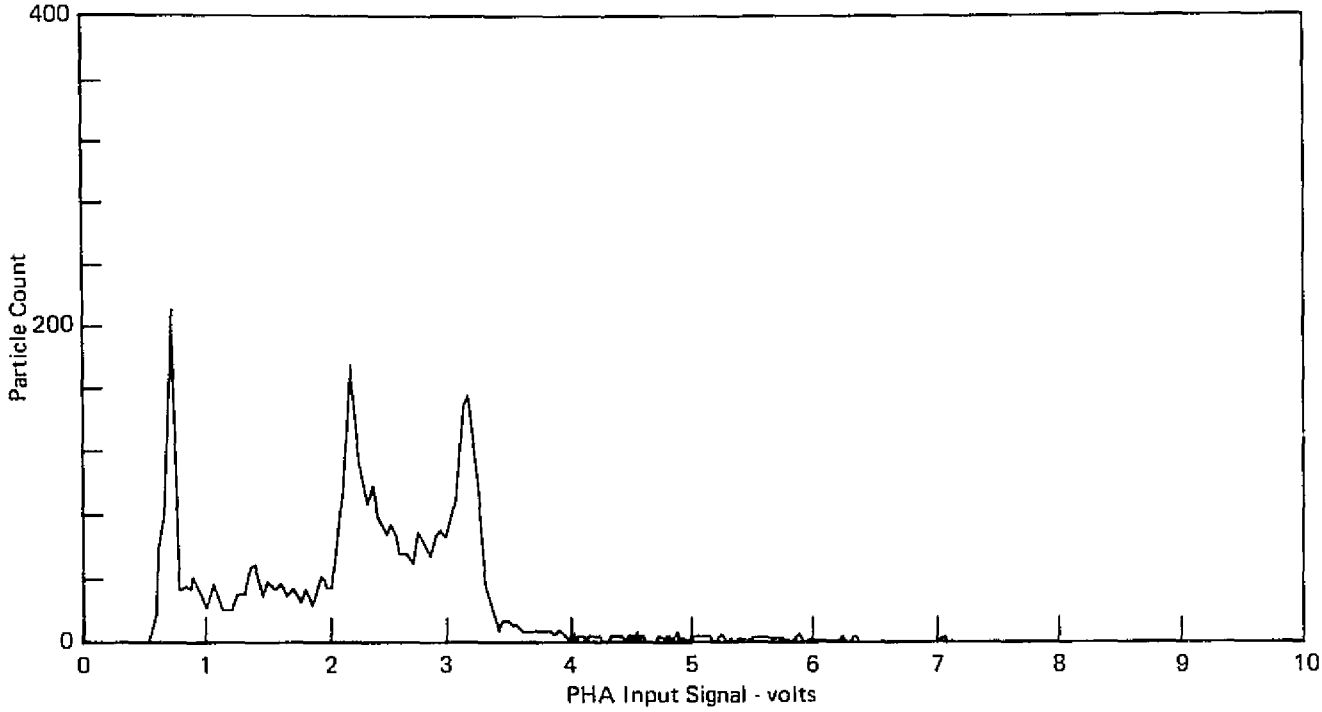

FIGURE 4-16 – EXTINCTION CHANNEL SIZE SPECTRUM
44-55 MICRON DIAMETER AND 88-105 MICRON DIAMETER GLASS BEADS

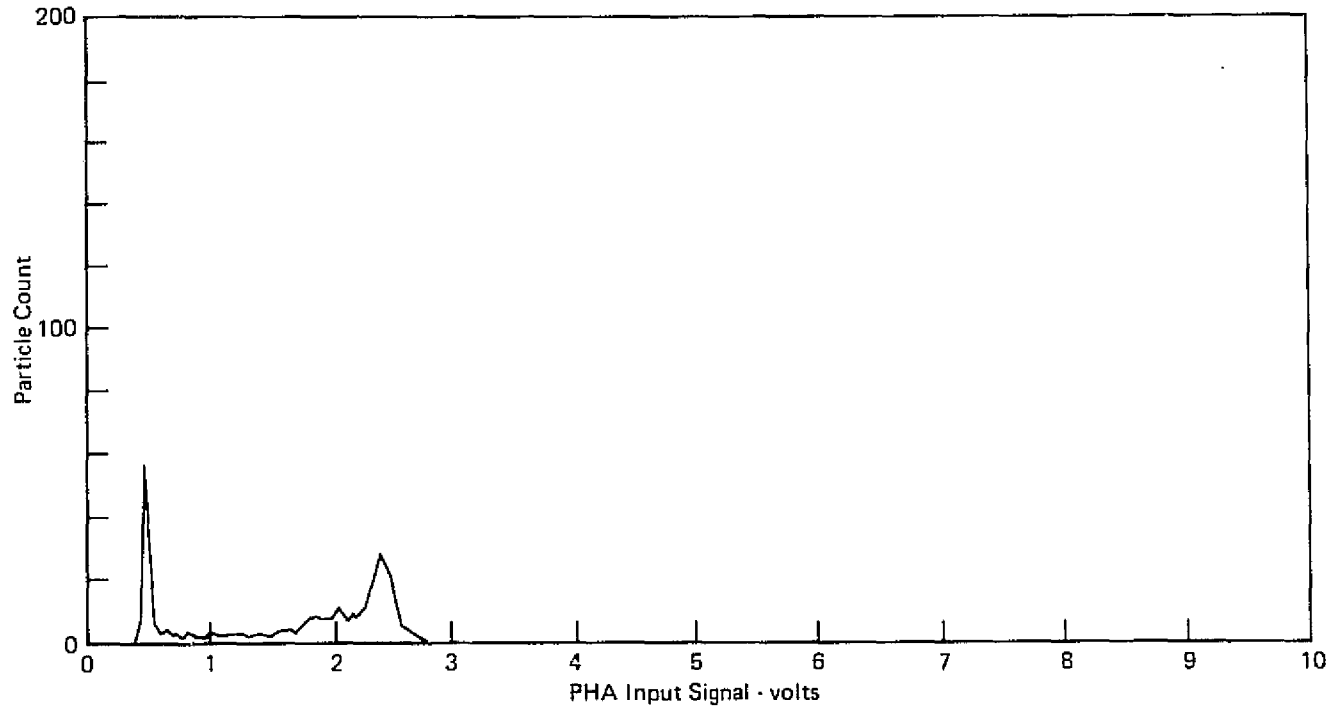

FIGURE 4-17 – EXTINCTION CHANNEL SIZE SPECTRUM
63-74 MICRON DIAMETER GLASS BEADS

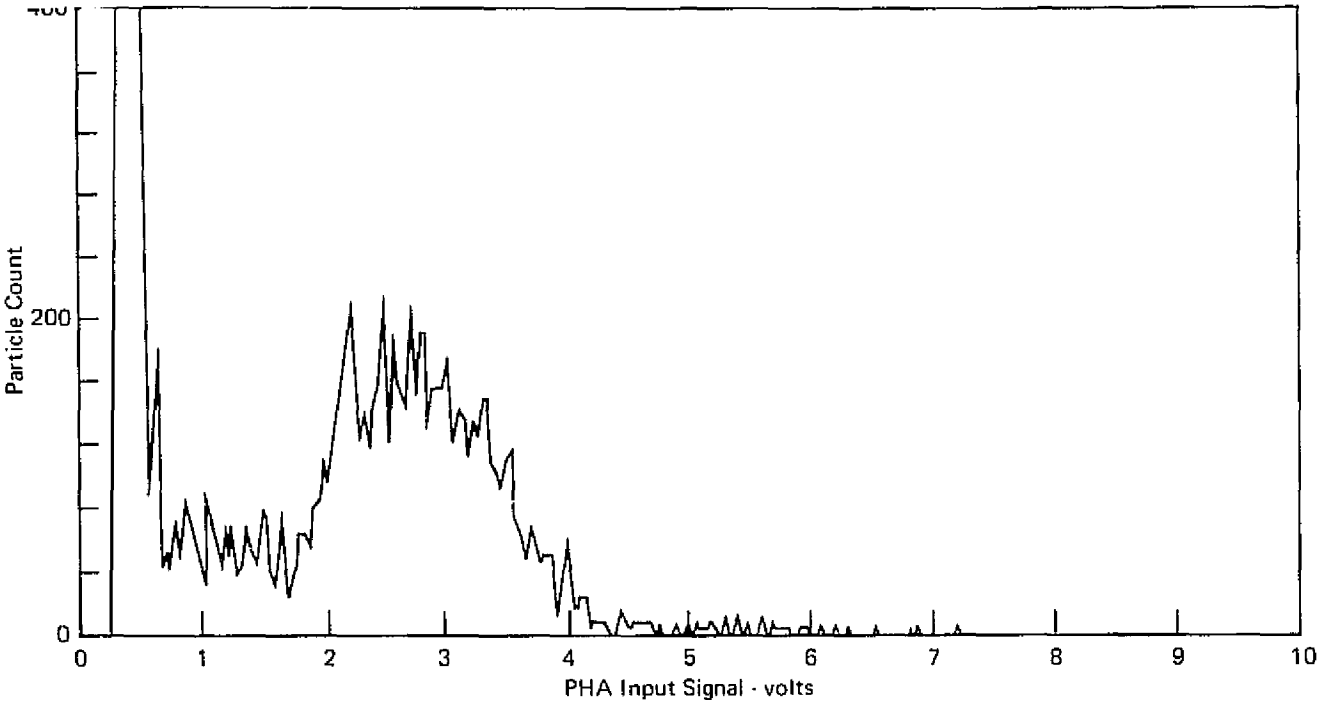

FIGURE 4-18— EXTINCTION CHANNEL SIZE SPECTRUM
44-53 MICRON DIAMETER GLASS BEADS

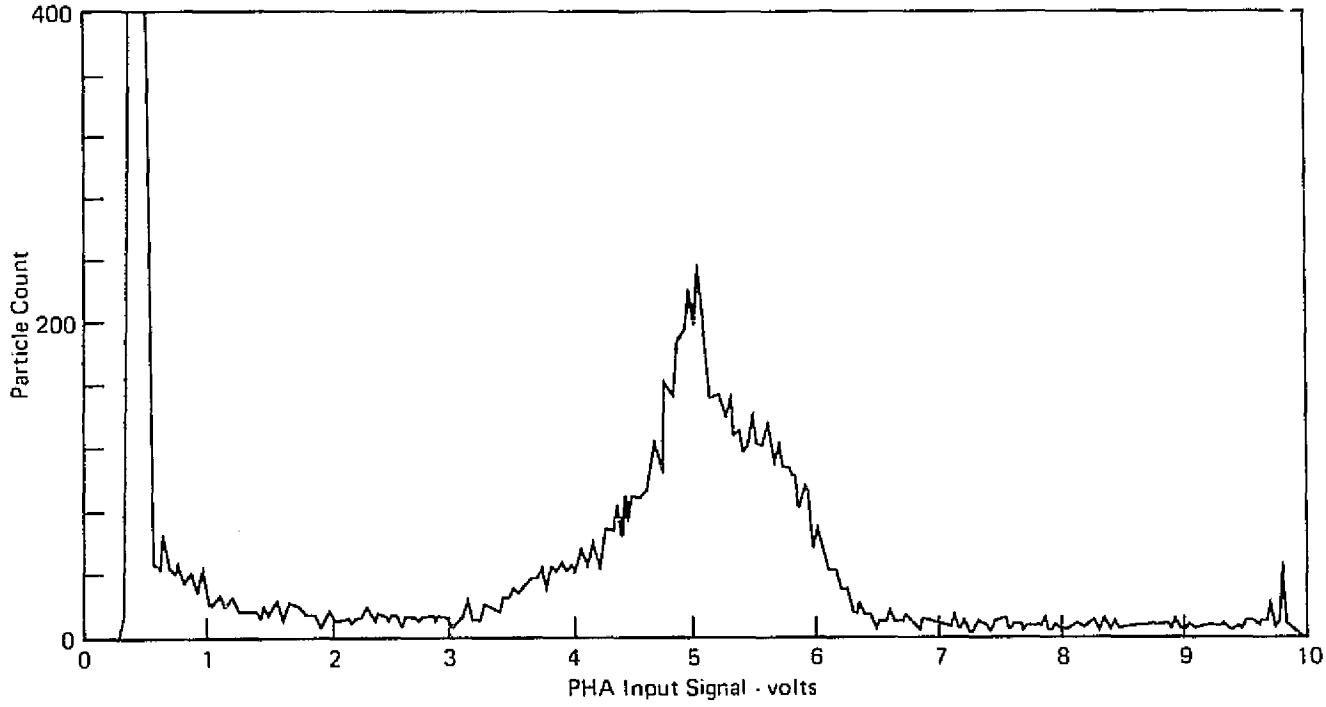

FIGURE 4-19— EXTINCTION CHANNEL SIZE SPECTRUM
125-150 MICRON DIAMETER GLASS BEADS

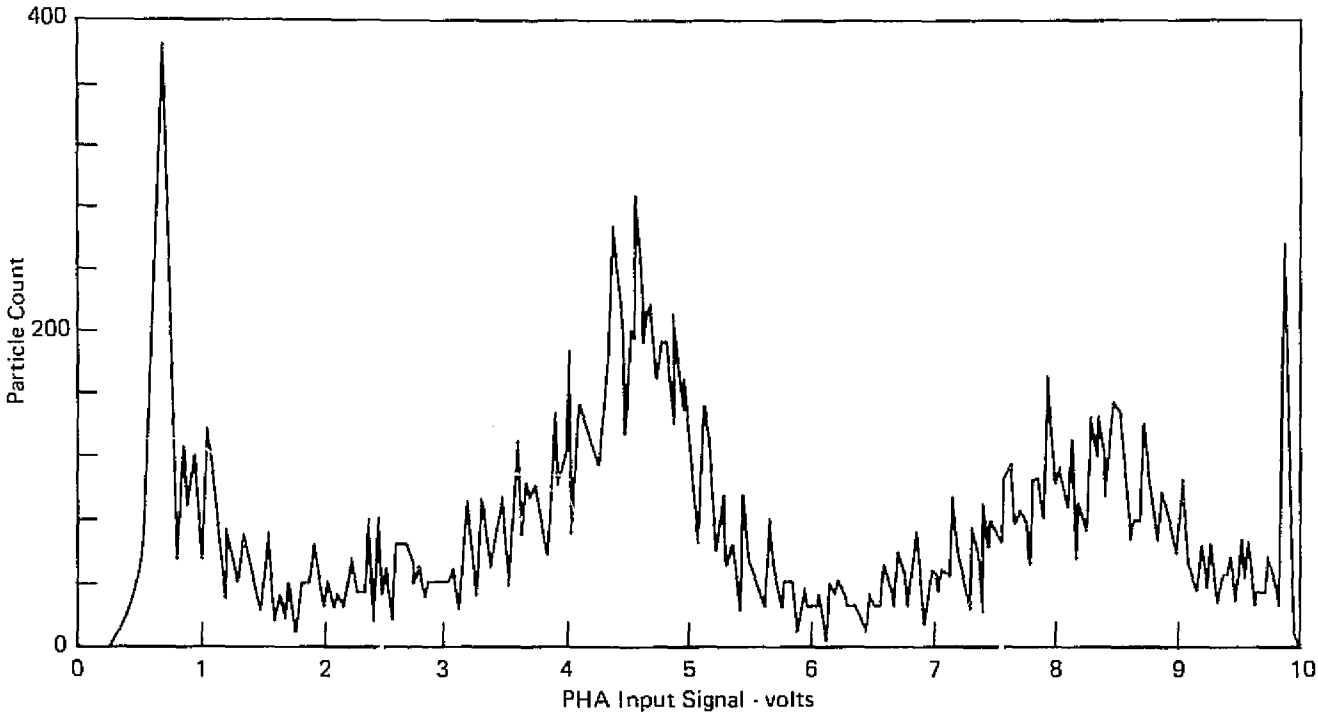

FIGURE 4-20 - EXTINCTION CHANNEL SIZE SPECTRUM
125-150 MICRON DIAMETER AND 200-250 MICRON DIAMETER GLASS BEADS

The extinction channel calibration derived from this data is shown in Figure 4-21. The boxes were constructed using the width (volts) of the PHA peak at half-height and the size range (microns) in which 90% of the particles are located. For example, the 200-250 micron glass beads produce a PHA peak in the 7.5 to 9 volt range (see Figure 4-20). The lower limit for this channel lies between 15 and 20μ diameter while the upper limit extends to approximately 275μ diameter. These data indicate that the gain of the scattering channel should be adjusted to obtain a span up to 20μ diameter in order to obtain sensitivity in the 10-20μ diameter range.

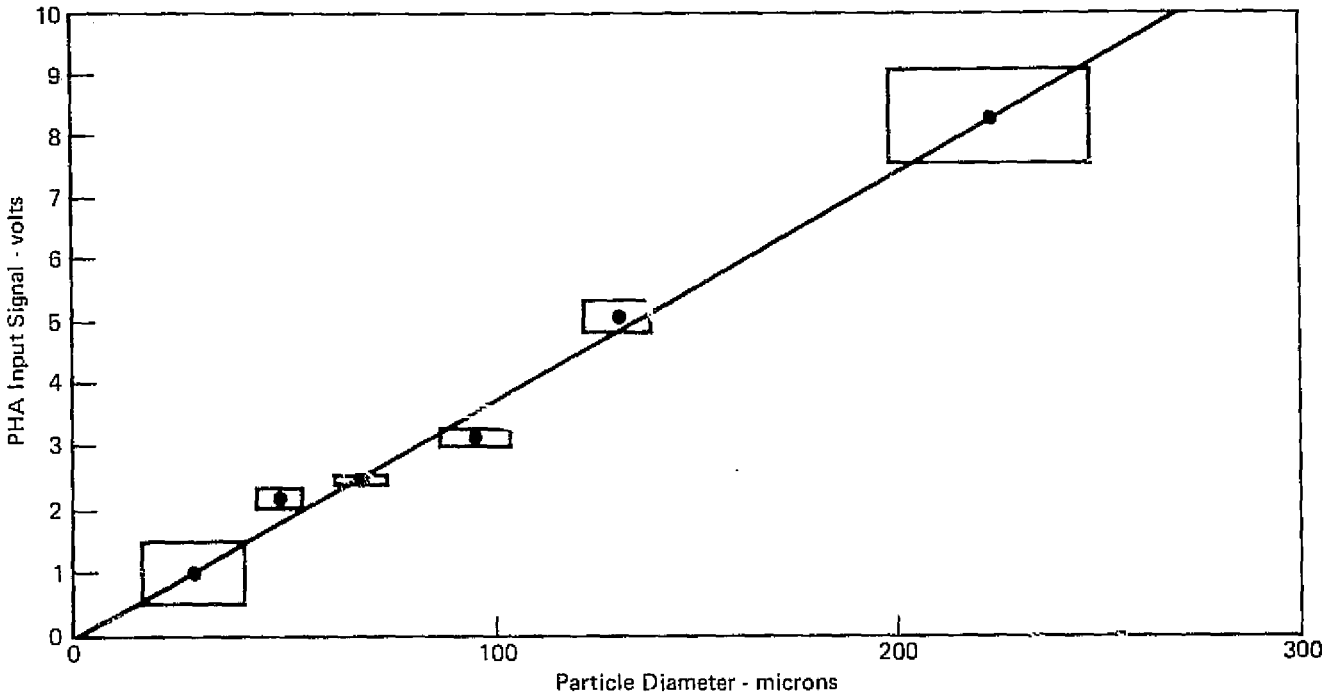

FIGURE 4-21 - EXTINCTION CHANNEL SIZE CALIBRATION

4.4.3 TRANSIT TIME CALIBRATION. Calibration of the scattering and extinction transit time spectra can be obtained in absolute terms since these spectra rely on the 1MHz internal clock in the Time-of-Flight (TOF) circuit. The TOF circuit output is +5 volts for zero transit time and decreases in a linear fashion to zero volts for a transit time equal to 8192μs (see Figure 4-22).

In terms of particle speed, the PHA 0-5 volt scale is highly non-linear. Linearization can be accomplished via the calculator software once the real-time data is recorded, as described in Volume II.

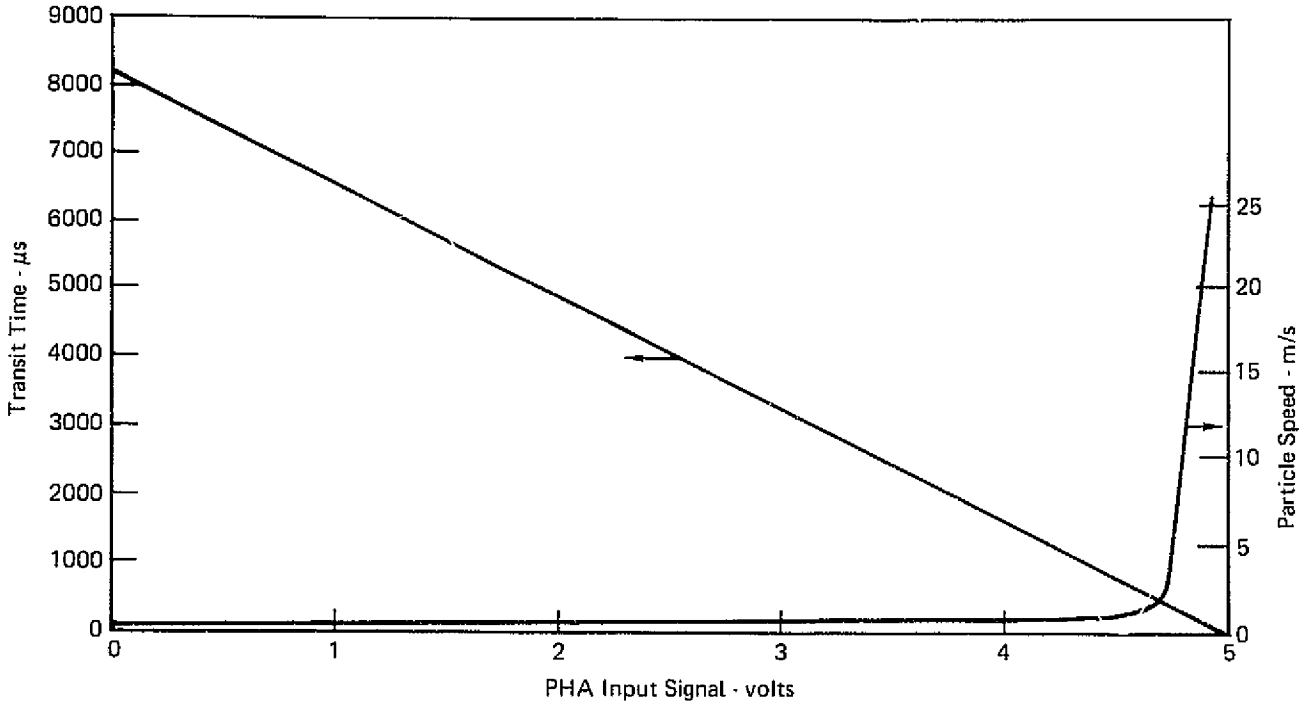

FIGURE 4-22– LPS TRANSIT TIME AND PARTICLE SPEED CALIBRATION

5.0 CONCLUSIONS AND RECOMMENDATIONS

This report has described the design and performance characteristics of a Laser Particulate Spectrometer (LPS) System, a proof-of-principle prototype instrument with demonstrated capability to measure the size and speed spectra of particulates from 0.8 to 275μ diameter, moving at speeds from 0.2 to 20m/second. System performance under vacuum conditions with cold shroud temperatures from 77 to 300°K was demonstrated. Successful electronic interfacing of the LPS System and the NASA-furnished Hewlett-Packard 5401B/9810 Multichannel Analyzer/Programmable Calculator System was accomplished via the LPS Electronics System and automatic system operation under program control was achieved. Verification of the design analysis was obtained by calibrating the LPS system with particulates of known size.

Experience gained thus far in LPS system operation has revealed several potential areas for improvement. It became evident that operation of the LPS in extremely dirty environments can cause occasional contamination of the laser mirrors and Brewster windows. In the most severe cases particulate contamination can cause a loss of the TEM_{01*} mode. Usually contamination is revealed by the gradual loss of laser beam intensity as the mirrors, lenses and windows become degraded. It is recommended that improvements in the design of the conical baffles be pursued, and an automatic gain compensation circuit be studied, as potential methods for reducing the effects of contamination on system performance.

It may be possible to reduce the overall size of the Sensor Head by studying alternatives to the helium-neon laser used in the present design.

The use of semiconductor injection laser diodes might be the key to eventual miniaturization of the Sensor Head.

6.0 BIBLIOGRAPHY

6.1 LIGHT SCATTERING TECHNIQUES

Anderson, W. L. and Beissner, R. E., "Counting and Classifying Small Objects by Far-Field Light Scattering", Appl. Opt. 10,1503 (1971).

Aughey, W. H. and Baum, F. J., "Angular Dependence Light Scattering - A High Resolution Recording Instrument...", J.O.S.A. 44,833 (1954).

Blau, H. H., Cohen, M. L., Lapson, L. B., von Thuna, P., Ryan, R. T., and Watson, D., "A Prototype Cloud Physics Laser Nephelometer", Appl. Opt. 9, 1798 (1970).

Cohen, A., "Comments on: Determination of Aerosol Size Dist. from Spectral Atten. Meas.", Appl. Opt. 11, 1657 (1972).

Chu, Chiao-Min, "Representation of the Angular Distribution of Radiation Scattered by a Spherical Particle", J.O.S.A. 45,958 (1955).

Dave, J. V., "Coefficients of the Legendre and Fourier Series for the Scattering Functions fo Spherical Particles", Appl. Opt. 9, 1888 (1970).

Dave, J. V., "Determination of Size Distribution of Spherical Polydispersions Using Scattered Radiation Data", Appl. Opt. 10,2035 (1971).

Dave, J. V., "Effect of Coarseness of the Integration Increment on the Calculation of the Radiation Scattered by Polydisperse Aerosols", Appl. Opt. 8,1161 (1969).

Deirmenjian, D., Electromagnetic Scattering on Spherical Polydispersions Elsevier, New York (1969).

Farmer, W. M., "Analysis of the Scattering Properties of Small Particles Under Coherent Multibeam Illumination", AF Contract F40600-73-C-0004, ARO Inc.

Grassl, H., "Determination of Aerosol Size Distributions from Spectral Attenuation Measurements", Appl. Opt. 10,2534 (1971).

Knollenberg, R. G., "An Active Scattering Aerosol Spectrometer", Atmos. Tech., No. 2 (June 1973).

Knollenberg, R. G., "Particle Size Measurements from Aircraft Using Electro-Optical Techniques", Proc. Electro-Optical Design Conference - 1971 West (May 18-20 1971).

Knollenberg, R. G., "The Study and Development of an Active Scattering Particle Size Spectrometer for Space Environments", NASA CR-12411 (1972), Contract NAS8-28297.

Letcher, J. H. and Schmidt, D. W., "Small Angle X-Ray Scattering Determination of Particle - Diameter Distributions in Polyd. Suspensions of Spherical Particles", J. Appl. Phys. 37,649 (1966).

Lind, A. C., "Aerosol Scattering Calculations", Memo MDRL-972 (2 July 1972).

McCormick, M. P. and Lawrence, J. D., Jr., "Tables of Mie Scattering Functions for Particles with Refractive Index 1.5", NASA TND-5110 (March 1969).

Mehta, N. K., Grimson, A., and Block, A. McB., "Effect of Dispersing Agents on the Angular Dependence of Light Scattered from Polystyrene Sphere/Water Sols", Appl. Opt. 10,2031 (1971).

Phillips, D. T. and Wyatt, P. J., "Single-Particle Light-Scattering Measurement: Photochemical Aerosols and Atmospheric Particulates", Appl. Opt. 11,2082 (1972).

Pinnick, Rosen, and Hofmann, "Measured Light-Scattering Properties of Individual Aerosol Particles Compared to Mie Scattering Theory", Appl. Opt. 12,37 (1973).

Roess, L. C., "A Simple Method of Obtaining a Particle Mass Distribution by Inverting the X-Ray Intensity Scattered at Small Angles", J. Chem. Phys. 14,695 (1946).

Rowell, R. L. and Stein, R. S., Electromagnetic Scattering, Gordon and Breach, New York (1967).

Ryan, Blau, Von Thuna, Cohen, and Roberts, "Cloud Microstructure as Determined by an Optical Cloud Particle Spectrometer", J. of Appl. Meteor. 11, 149 (1972).

Shahrokhi, F. and Wolf, P., "Mie Scattering Function", NASA CR-1022.

Sinclair, D., "Light Scattering by Spherical Particles", J.O.S.A. 37,475 (1947).

Twomey, S. and Howell, H. B., "Some Aspects of the Optical Estimation of Microstructure on Fog and Cloud", Appl. Opt. 6,2125 (1967).

Van De Hulst, H. C., Light Scattering by Small Particles, John Wiley and Sons, Inc., New York (1957).

Westwater, E. R. and Cohen, A., "Application of Backus-Gilbert Inversion Technique to Determination of Aerosol Size Distributions from Optical Scattering Meas.", Appl. Opt. 12,1340 (1973).

Willard, G. W., "Criteria for Normal and Abnormal Ultrasonic Light Diffraction Effects", J. Acoustical Soc. of Amer. 21,101 (1949).

Williams, J. R. and Russell, D. M., "Particle Analysis by Active Scattering Particle Spectrometry", S&E-SSL-P, Ph-205-453-0941 (1972).

Wyatt, P. J., "Differential Light Scattering: A Physical Method for Identifying Living Bacterial Cells", Appl. Opt. 7,1879 (1968).

6.2 INTRA-CAVITY LASER TECHNIQUES

Meehan, E. J. and Gyberg, A. E., "Particle Size Determination by Low-Angle Light Scattering: Effect of Refractive Index", Appl. Opt. 12,551 (1973).

Rigrod, W. W., "Gain Saturation and Output Power of Optical Masers", J. Appl. Phys. 34,2602 (1963).

Proctor, T. D., "A Laser Technique for the Measurement of Aerosols", J. Phys. E1, 631 (1968).

Schehl, R. Ergun, S. and Headrick, A., "Size Spectrometry of Aerosols Using Light Scattering from the Cavity of a Gas Laser", RSI 44,1193 (1973).

Schleusener, S. A., "Automatic High Speed Particle Sizing Using a Gas Laser", RSI 39,1916 (1968).

Schleusener, S. A. and Read, A. A., "Variable Brewster Angle Flat Used as a Gas Laser Gain Control", RSI 37,287 (1966).

Schuster, B. G. and Knollenberg, R. "Detection and Sizing of Small Particles in an Open Cavity Gas Laser", Appl. Opt. 11,1515 (1972).

Stark, H., "Comments On: Particle Size Analyzer", Appl. Opt. 11,1655 (1972).

6.3 IMAGING TECHNIQUES

Ballik, E. A. and Chan, J. H. S., "Fringe Image Technique for the Measurement of Flow Velocities", Appl. Opt. 12,2607 (1973).

Chan J. H. C. and Ballik, E. A., "Application of Fourier Images to the Measurement of Particle Velocities", Appl. Opt. 13,234 (1974).

Dotson, W. P., Jr., "The Effect of Object Motion in Fraunhofer Holography with Application to Velocity Measurements", NASA TND-5515 (November 1969).

Knollenberg, R. G., "Comparative Liquid Water Content Measurements of Conventional Instruments with an Optical Array Spectrometer", J. Appl. Meteor. 11,501 (1972).

Knollenberg, R. G., "The Optical Array: An Alternative to Scattering or Extinction for Airborne Particle Size Determination", J. Appl. Meteor. 9,86 (1970).

Mayo, W. T., Jr., and Allen, J. B., "New Doppler Holographic Technique for Fluid Velocity Visualization and Measurement", Appl. Opt. 10,2119 (1971).

McSweeney, A. and Rivers, W. "Optical-Fiber Array for Measuring Distributions of Light Intensity for Particle Size Analysis", Appl. Opt. 11,2101 (1972).

6.4 LASER DOPPLER VELOCIMETRY

Angus, J. C., Morrow, D. L., Dunning, J. W., Jr., and French M. J., "Motion Measurement by Laser Doppler Techniques", Ind. Eng. Chem. 61,9 (1969).

Avidor, J. M., "Novel Instantaneous LDV", Appl. Opt., 13,280 (1974).

Brayton, D. B., Kalb, H. T., and Crosswy, F. L., "Two-Component Dual-Scatter Laser Doppler Velocimeter with Frequency Burst Signal Readout", Appl. Opt. 12,1145 (1973).

Cliff, W. C., Fuller, C. E. and Sandborn, V. A., "Simultaneous Comparison of Turbojet Gas Fluctuations by Laser Doppler and Hot Wire", IAAA Journal 11,748 (1972).

Crosswy, F. L. and Hornkohl, J. O., "Signal Conditioning for a Laser Vector Velocimeter", RSI 44,1324 (1973).

Dandliker, R. and Iten, P. D., "Direction Sensitive Laser Doppler Velocimeter with Polarized Beams", Appl. Opt. 13-286 (1974).

Davies, W. E. R., "Velocity Measurements in Bubbly Two-Phase Flows Using Laser Doppler Anemometry", (Part I), UTIAS TN No. 184 (Jan 1973).

Denison, E. B. and Stevenson, W. H., "Oscillatory Flow Measurements with a Directionally Sensitive Laser Velocimeter", RSI 41,1475 (1970).

Durst, F., et al, "Lectures for International Short Coarse on Laser Velocimetry", PDU Lectures 74C29 (25-29 March 1974).

Farhat, N. H. and Weiskittel, H. M., "Determination of the Velocity Vector of Point Retroreflectors by Spatial Filtering of Doppler Spectra", Appl. Opt. 10,868 (1971).

Farmer, W. M., "Determination of a Third Orthogonal Velocity Component Using Two Rotationally Displaced Laser Doppler Velocity Systems", Appl. Opt. 11,770 (1972).

Farmer, W. M. and Hornkohl, J. D., "Two-Component, Self Aligning Laser Vector Velocimeter", Appl. Opt. 12,2637 (1973).

Farmer, W. M., Hornkohl, J. O., and Brayton, D. B., "A Relative Performance Analysis of Atmospheric LDV Methods", Opt. Eng. Vol. II, No. 1, p. 24 (January/February 1972).

Foreman, W. and Huffaker, R. M., "Development of a Laser Doppler Flowmeter for Gas Velocity Measurement", NASA TMX-53389 (1966).

Fridman, J. D., Huffaker, R. M., and Kinnard, R. F., "Laser Doppler System Measures Three-D. Vector Velocity and Turbulence", Laser Focus, (November 1968).

Fuller, C. E., Cliff, W. C. and Huffaker, R. M., "Three-Dimensional LDV Turbulence Measurements in a Pipe Flow", NASA CR-129017 (April 1973).

Grant, G. R. and Donaldson, R. W., "A Laser Velocity Measurement System for High-Temperature Wind Tunnels", NASA TMX-1976 (April 1970).

Grant, G. R. and Orloff, K. L. "Two-Color Dual-Beam Backscatter Laser Doppler Velocimeter", Appl. Opt. 12,2913 (1973).

Gollub, J. P., Chabay, I. and Flygare, W. H., "Optical Hetrodyne Measurement of Cloud Droplet Size Distribution", Appl. Opt. 12,2838 (1973).

Karchmer, A. M., "Particle Trackability Considerations for Laser Doppler Velocimeters", NASA TMX-2628 (September 1972).

Lading, L., "Differential Doppler Hetrodying Technique", Appl. Opt. 10,1943 (1971).

Lanz, O., Johnson, C. C., and Morikawa, S., "Directional Laser Doppler Velocimeter", Appl. Opt. 10,884 (1971).

Mayo, W. T., "Simplified Laser Doppler Velocimeter Optics", J. Phys. E3,325 (1970).

Mazumder, M. K., "A Symmetrical Laser Doppler Velocity Meter and It's Application to Turbulence Characterization", NASA CR-2031 (May 1972).

Meyers, J. F., "Investigation and Calculations of Basic Parameters for the Application of the LDV", NASA TND-6125 (April 1971).

Meyers, J. F., "Investigation of Basic Parameters for the Application of a LDV", AIAA 71-288 (April 1971).

Orloff, K. L. and Grant, G. R., "The Application of a Scanning Laser Doppler Velocimeter for Trailing Vortex Definition and Alleviation", AIAA 73-680 (1973).

Owens, J. C., "Comment on - Analysis of Atmospheric LDV", Appl. Opt. 11,2977 (1972).

Rudd, M. J., "The Laser Anemometer: A Review", Optics and Laser Tech., p. 200, (November 1971).

Rudd, M. J., "A New Theoretical Model for the Laser Dopplermeter", J. Phys. E2,55 (1969).

Uzgiris, E. E., "Laser Doppler Spectrometer for Study of Electrokinetic Phenomena", RSI 45,74 (1974).

von Stein, H. D. and Pfeifek, H. J., "Investigation of the Velocity Relaxation of Micron Sized Particles in Shock Waves Using Laser Radiation", APPL. Opt. 11,305 (1972).

Wang, C. P., "New Model for Laser Doppler Velocity Measurement on Turbulent Flow", App. Phys. Lett. 18,522 (1971).

Wang, C. P., "A Unified Analysis on Laser Doppler Velocimeters", J. Phys. E 5,763 (1972).

Wang, C. P. and Snyder, D., "Laser Doppler Velocimetry: Experimental Study", Appl. Opt. 13,98 (1974).

Yanta, W. J., Gates, D. F. and Brown, F. W., "The Use of a Laser Doppler Velocimeter in Supersonic Flow", AIAA 71-287 (March 1971).

6.5 MISCELLANEOUS LASER TECHNIQUES

Cornillault, J., "Particle Size Analyzer", Appl. Opt. 11,265 (1972).

Farmer, W. M., "Measurement of Particle Size, Number Density, and Velocity Using a Laser Interferometer", Appl. Opt. 11,2603 (1972).

Farmer, W. M., "Observation of Large Particles with a Laser Interferometer", Appl. Opt. 13,610 (1974).

McCormick, M. P., "Laser Backscatter Measurements of the Lower Atmosphere", Wm. and Mary Thesis (Physics) 67A01.

She, C. Y., "Laser Cross-Beam Intensity - Correlation Spectrum for a Turbulent Flow", Appl. Opt. R,2415 (1973).

Siegman, A. E., An Introduction to Lasers and Masers, McGraw Hill, New York (1971).

Silverman, B. A., Thompson, B. J., and Ward, J. H., "A Laser Fog Disdrometer", J. Appl. Meteor. 3,792 (1964).

"Laser System Detects Clean Room Contamination", Laser Focus (November 1968).

6.6 MISCELLANEOUS OPTICAL TECHNIQUES

Clarke, W. B., "Liquid Velocity Measurements by Electronic Detection of Particle Images", MIT (Chem. Eng.),P/R 68 H04 (1968).

Martens, A. E., "An Electro-Optical Part,Counter", Bausch and Lomb, Inc., (February 1966).

Martens, A. E and Doonan, D. D., "Comments On: Influence of Refractive Index on the Accuracy of Size Determination of Aerosol Particles with Light-Scattering Aerosol Counters", Appl. Opt. 9, 1930 (1970).

Moroz, with Standley and Anderson, "A Portable Counter and Size Analyzer for Airborne Parts", RSI 41,978 (1970).

Pinnick, R. G. and Hofmann, D. J., "Effeciency of Light Scattering Aerosol Particle Counters", Appl. Opt. 12,2593 (1973).

Reagan, J. A. and Herman, B. M. "Three Optical Methods for Remotely Measuring Aerosol Size Distribution", AIAA 71-1057.

Schwar, M. J. R., "Doppler Velocity Measurements Using White Light", Nature 229,621 (1971).

Wang, C. P., "Doppler Velocimeter Using Diffraction Grating and White Light", Appl. Opt. 13,1193 (1974).

6.7 MISCELLANEOUS PARTICLE SIZING TECHNIQUES

Blanchard, Farlow, and Ferry, "Methods of Analyzing Microsize Particulate Aerosols and Contaminants", AIAA 71-1104.

Carr, Brion and Jenkinson, "X-Ray, Flourescence Particle Sizing", Appl. Opt 12,449 (1973).

Mit ., Jacchia, and Newman (Ed.), Cospar Space Research VIII, North Holland, Amsterdam, (1968).

Twomey, S. and Severynse, G. T., "Measurement of Size Distributions of Natural Aerosols", J. Atmos. Sci. 20,392 (1963).

Symposium on Particle Size Measurement, ASTM Special Tech. Pub. #234 (1959).

6.8 AEROSOLS AND THEIR GENERATION

Denton, M. B. and Swartz, D. B., "An Improved Ultrasonic Nebulizer System for the Generation of High Density Dispersions", RSI 45,81 (1974).

Hidy, G. M., Editor, Aerosols and Atmospheric Chemistry, Academic Press, New York (1972).

Kuhn, W. E., Lamprey, H. and Sheer, C., Ultrafine Particles, Wiley, New York (1963).

Mercer, T. T., Morrow, P. E., and Stober, W., Assessment of Airborne Particles, C. C. Thomas, Springfield, Illinois, (1972).

Vonnegut, B. and Neubauer, K. L., "Production of Monodisperse Liquid Particles by Electrical Atomization", J. of Coll. Sci. 7, 616 (1952).

6.9 VACUUM-QUALIFIED LASERS

Kolb, N. P., "Research Directed Toward Perfecting a Design for a Space-Qualified He-Ne Laser - Interim Report", Hughes Aircraft Co., Electron Dynamics Division, Torrance, Cal., to NASA Contract NAS12-579, (Jan 1969, and Jan 1970).

7.0 REFERENCES

(1) O. Hamberg "Photographic Measurement of Particulate Surface Contamination" NASA SP-336, Nov. 1973 p. 379.

(2) H. K. F. Ehlers, R. G. Richmond, J. T. Visentine "Determination of a High Velocity Water-Vapor Plume Profile in a Thermal Vacuum Environment," NASA SP-336, Nov. 1973 p. 727.

(3) H. K. F. Ehlers, A. Lee, J. Robertson, "Mathematical Model of Molecular Flow in the NASA-JSC Thermal Vacuum Chamber A", NASA SP-336, Nov. 1973 p. 757.